Surface (sea floor) and near-surface (box cores) sediment mineralogy in Baffin Bay as a key to sediment provenance and ice sheet variations

John T. Andrews and D.D. Eberl

Abstract: To better understand the glacial history of the ice sheets surrounding Baffin Bay and to provide information on sediment pathways, samples from 82 seafloor grabs and core tops, and from seven box cores were subjected to quantitative X-ray diffraction weight percent (wt.%) analysis of the <2 mm sediment fraction. The samples were collected between 67°N and 78°N, in water depths of 155 to 2375 m and were retrieved on cruises between A.D. 1964 and 2009. Grain size, magnetic characteristics, and colour reflectance data were also obtained on many of the samples. Twenty-one non-clay and 10 clay mineral species were identified; the average wt.% of the non-clay minerals was 70% and was dominated by quartz, various feldspars, and dolomite, whereas the dominant clay minerals were 1 M illite, biotite, and chlorite. Cluster analysis on principal component scores identified three main mineral groups, which also had strong associations with grain size and sediment magnetic properties. Box cores from the deep central basin (>2000 m) all show an abrupt drop in calcite wt.% (post-5 cal ka BP?) following a major peak in detrital carbonate (mainly dolomite). This dolomite-rich detrital carbonate (DC) event in JR175BC06 is possibly coeval with the Younger Dryas cold event. Four possible glacial-sourced end members were employed in a compositional unmixing algorithm to gain insight into down core changes in sediment provenance at the deep central basin. Estimates of the rates of sediment accumulation in the central basin are only in the range of 2 to 4 cm/cal ka, surprisingly low given the glaciated nature of the surrounding land.

Résumé : Afin de mieux comprendre l'historique glaciaire des inlandsis autour de la baie de Baffin et de fournir de l'information sur les chemins pris par les sédiments, des échantillons de quatre-vingt-deux (82) prélèvements de fond océanique au hasard et de sommets de carottes et de sept (7) carottiers à boîte ont été soumis à des analyses de rayons-X quantitatives de pourcentage poids sur la fraction des sédiments inférieure à 2 mm. Les échantillons ont été prélevés entre les latitudes 67 et 78°N à des profondeurs entre 155 et 2375 m et ils ont été récupérés lors de croisières entre 1964 et 2009. Des données sur la granulométrie, les caractéristiques magnétiques et la réflexion de la couleur ont aussi été obtenues sur plusieurs échantillons. Vingt et une (21) espèces minérales non argileuses et dix espèces minérales argileuses ont été identifiées; le pourcentage poids moyen des minéraux non argileux était de 70 % et ils étaient composés surtout de quartz, de divers feldspaths et de dolomite alors que les minéraux argileux dominants étaient 1M illite, biotite et chlorite. Une analyse par grappes des cotes des principales composantes a permis d'identifier trois principaux groupes minéraux, lesquels étaient aussi fortement associés aux propriétés granulométriques et magnétiques des sédiments. Les sédiments prélevés par des carottiers à boîte dans le bassin central profond (>2000 m) montraient tous une chute abrupte du pourcentage poids de la calcite (plus récent que 5 ka cal. avant le présent?) après une crête significative de carbonate détritique (surtout de la dolomite). Cet événement de carbone détritique riche en dolomite dans l'échantillon JR175BC06 est peut-être contemporain de la période froide du Dryas récent. Quatre membres terminaux possiblement de source glaciaire ont été utilisés dans un algorithme de démêlage compositionnel dans le but de mieux comprendre les changements de source des sédiments en profondeur dans les carottes provenant du bassin central profond. Des estimations des taux d'accumulation de sédiments dans le bassin central ne sont que de l'ordre de 2 à 4 cm/ka cal., étonnamment faible étant donné la nature glaciée du terrain environnant.

[Traduit par la Rédaction]

Received 4 October 2010. Accepted 14 March 2011. Published at www.nrcresearchpress.com/cjes on 19 August 2011.

Corresponding Editor: David Scott.

J.T. Andrews. INSTAAR and Department of Geological Sciences, University of Colorado, Box 450, Boulder, CO 80309, USA.
D. Eberl. US Geological Survey, 3215 Marine Street, Suite E-127, Boulder, CO 80303, USA.

Corresponding author: John T. Andrews (e-mail: andrewsj@colorado.edu).

Introduction

Baffin Bay is, and certainly was, one of the most heavily impacted ocean basins during the late Cenozoic glaciations (Aksu 1981; Hiscott et al. 1989; Srivastava et al. 1989). Baffin Bay is a 689 000 km^2 ocean basin with a northern link to the Arctic Ocean via the Canadian High Arctic channels and a southern link to the Labrador Sea and the North Atlantic via Davis Strait (Tang et al. 2004; Fig. 1). The deep central basin attains water depths of ~2500 m. The surface circulation is anti-clockwise with modified Atlantic Water being advected northwards along West Greenland (WG), whereas on

the Baffin Island (BI) side, cold, ice-laden Polar Waters move southward in the Baffinland Current, joining with the outflow from Hudson Bay – Hudson Strait to form the Labrador Current. On the eastern side, the Greenland Ice Sheet sheds icebergs and meltwater into the fiords and continental shelf. In the 1970s, it was estimated that some 40 000 icebergs are calved per year into Baffin Bay (Jacobs et al. 1985), with an estimated annual flux of between 100 and 150 km^3/year (Bigg 1999), although the calving flux might have increased in recent years (Howat et al. 2007) as has the meltwater flux (Hanna et al. 2008).

Studies of the lithofacies and mineralogy of the late Quaternary sediments in Baffin Bay and nearby areas have been reported, starting mainly in the 1960s (Kranck 1966; Marlowe 1966), with later major contributions by Piper, Aksu, and colleagues (Piper 1973; Boyd and Piper 1976; Aksu and Piper 1987; Andrews et al. 1998). Ocean Drilling Program (ODP) site 645 was also drilled in deep water toward the western margin of the Bay (Fig. 1 — near site BX14) with a focus on longer time scales (Hiscott et al. 1989). A fundamental feature of the Quaternary stratigraphy in Baffin Bay is the presence of discrete, detrital carbonate (DC) lithofacies (Piper 1973; Aksu 1981). Data from Kane Basin and Smith Sound add additional information on the distribution of DC facies (Kravitz and Sorensen 1970; Kravitz 1982). In total, these earlier contributions demonstrated the importance of detrital carbonate events and also documented variations in clay-size mineralogy.

The purpose of the present paper is to add to this body of knowledge by providing an analysis of quantitative X-ray diffraction (qXRD) wt.% data on the <2 mm sediment fraction on grab samples obtained on various cruises of the Canadian research vessel CSS *Hudson*, with major collections in 1964, 1977, 1980, and 2008 (Fig. 1; Appendix A, Table A1). Box cores were collected in 2008 on HU2008029 and in 2009 on cruise JR175 (Sir James Clark Ross; Fig. 1); they have been studied to examine relatively short-term fluctuations in sediment compositions. In addition to these data, we also provide new data on grain size, magnetic variables, and colour reflectance on dried samples. A major objective is to see whether these data provide useful information on sediment composition and transport pathways.

Background

Bedrock geology

The bedrock geology of the area that contributes sediments into Baffin Bay is complex and difficult to portray on a simple map (MacLean 1985; MacLean et al. 1990; Jackson and Berman 2000). The Precambrian Shield, which forms the bulk of the outcrop in Greenland and Baffin Island, was rifted during the early Tertiary, with basalts of this age cropping out along both margins of the rift in the vicinity of Disko Island and Cape Dyer (Fig. 2, Tv; MacLean et al. 1990; Skaarup et al. 2006). Paleozoic limestone and dolomite floor the large rift channels and sounds that fringe northern Baffin Bay (Fig. 2) and on either side of Kane Basin (Fig. 2; Kravitz 1976, 1982) and are principally dolomites of different maturities (Parnell et al. 2007) but with some limestone and chert (Reid et al. 2008). Upper Cretaceous strata have also been identified on the Baffin Island shelf between 70°N and 72°N (Praeg et al. 2006) and in the grabens south of Davis Strait, Cretaceous mudstones outcrop below the Quaternary sediment cover (MacLean 1985, 2001; MacLean et al. 1986). The troughs that cut across the shelves (Fig. 1) have eroded through Cretaceous and Tertiary sediments, but they have limited outcrop at the seafloor because of the cover of Quaternary sediments (e.g., Praeg et al. 2006).

The Archaean and Paleoproterozoic rocks on either side of Baffin Bay form the largest bedrock outcrop and range in age from ca 3.8 to 1.825 Ga, with the major boundaries oriented SW–NE across the Bay (Jackson and Berman 2000). Hence, some Quaternary sediment provenance assignments may be possible based on their radiogenic isotopic values (Farmer et al. 2003). Based on the bedrock geology, we would expect that glacial erosion of the Archaean and Paleoproterozoic bedrock would supply large quantities of quartz and K-feldspars: there are limited outcrops of mafic bedrock in the vicinity of Disko Island (WG) and Cape Dyer (BI) but with a more extensive outcrop offshore (MacLean et al. 1990; Skaarup et al. 2006; Fig. 2). Erosion and transport of the Paleozoic carbonates would provide calcite, dolomite, and chert. Clay minerals, such as kaolinite and smectite, should be scarce as there is only limited surface outcrops of Cretaceous and Tertiary sediments north of Davis Strait (MacLean et al. 1990; Praeg et al. 2006; Fig. 2), but they might be transported into the bay by northward flowing surface and subsurface currents (Fagel et al. 2004).

Ocean circulation, sea ice, and icebergs

The ocean surface circulation in Baffin Bay is counterclockwise with relatively warm modified Atlantic Water being transported northward along the coast of WG in the West Greenland Current (WGC) and cold, relatively fresh Polar Water being directed southward in the Baffinland Current (Fig. 2; Tang et al. 2004). The surface waters are quite corrosive, especially on the western side of Baffin Bay, and the calcium compensation depth is shallow (Azetsu-Scott et al. 2010).

The prevailing ocean and atmospheric circulation makes for a pronounced asymmetry in the number of ice-free days across Baffin Bay (Crane 1978). The ice margin for July 2nd (average of 1971–2000; Fig. 2) trends nearly south–north with open water along the coast of West Greenland up to about 73°N, land-fast ice along much of the Baffin Island coast, and with drifting pack ice farther offshore. Sea ice, especially land-fast ice and heavy pack ice, hinders and even prevents the drift of icebergs, especially from December through March. In exceptionally severe years, sea ice can be brought along the WG coast from the south in the East Greenland Current (Schmith and Hansen 2003; the so-called "storis").

By-and-large, the sea ice in Baffin Bay is first year ice, although occasional floes of multi-year ice enter Baffin Bay from the ice-choked High Arctic channels. Kwok et al. (2010) estimated that between 150–250 km^3 of ice moved south toward Baffin Bay through Nares Strait (Fig. 2). The relative scarcity of beaches and shallow banks around Baffin Bay limits the entrainment of sediments by sea ice. However, the sea ice at fiord heads often has a cover of wind-blown sand, although much of this sediment load is probably shed within the fiord (Gilbert 1990).

Fig. 1. Location map showing the location of the surface (seafloor) grab samples (open circles) and the location of the box cores (BX, cruise HU2008029; BC, cruise JR175) and three piston cores. Letters refer to location of major troughs and ice streams: SI, Scott Inlet; HB, Home Bay; LS, Lancaster Sound; JS, Jones Sound; SS, Smith Sound; U, Umanak Trough; J, Jakobshavn Trough.

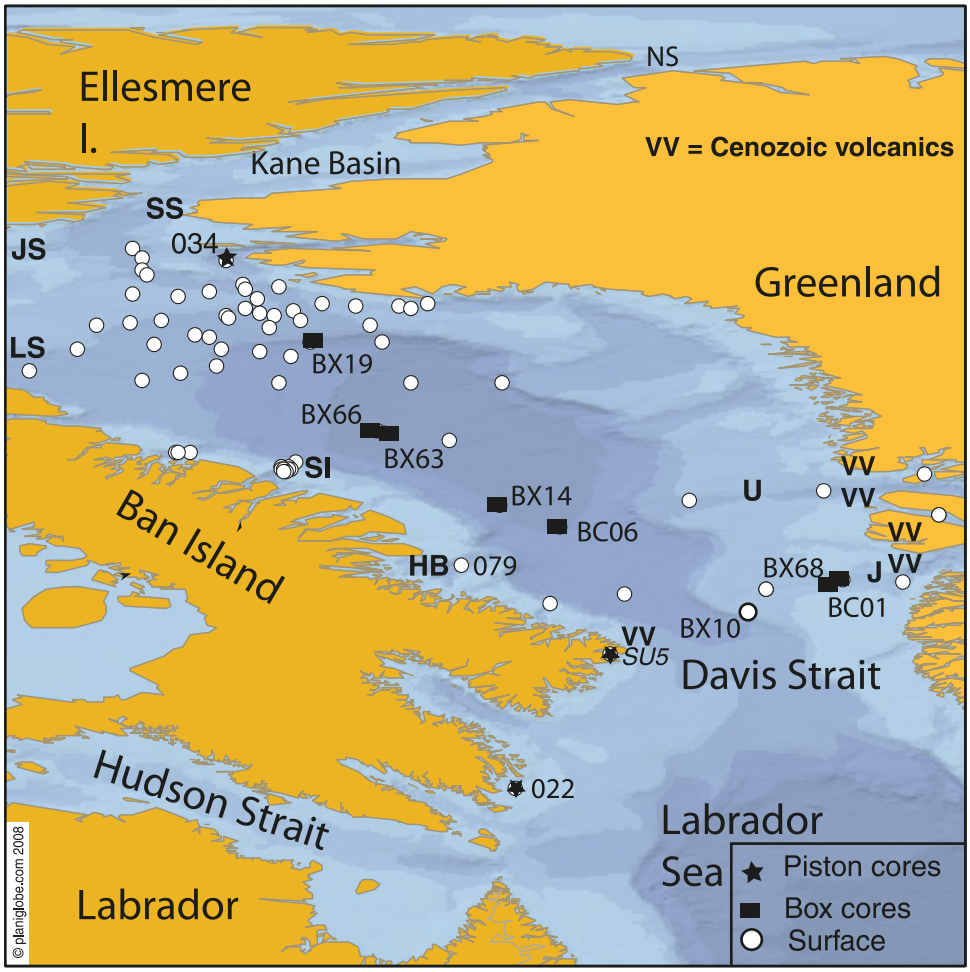

Baffin Island has few glaciers that reach tidewater and the vast bulk of icebergs that transit Baffin Bay are derived from fast-flowing outlets of the Greenland Ice Sheet (GIS; Bigg et al. 1996; Bigg 1999; Weidick and Bennike 2007), with some contribution from tidewater glaciers on the Canadian High Arctic islands. There is no yearly systematic count of iceberg numbers in Baffin Bay, although the International Ice Patrol has a 100-year record of the number of icebergs that cross 48°N off the coast of Labrador. Reeh (1994), Bigg (1999), and Weidick and Bennike (2007) have estimated the calving fluxes for individual West and NW Greenland ice streams (Fig. 2), with the total flux being in the range of 100–150 km^3 year. The fate of an iceberg depends in part on its draught and the water depth at the grounding line; if the keel depth is greater than the depth of sill at the fiord mouth then the icebergs are retained within the fiord until sufficient melting has occurred to allow passage onto the shelf. However, deep-keeled icebergs (>200 m draught) cannot traverse shallow banks and shelves.

There is little or no quantitative information on the sediment load of icebergs. Most icebergs are calved at the tidewater margins of fast-flowing ice streams or glaciers; hence we can expect that the vast bulk of the sediment is a 10 m or so thick basal unit (Dowdeswell 1986; Alley et al. 1997; Andrews 2000), which would probably melt out rapidly, especially in the presence of Atlantic Water (Holland et al. 2008). Thus, only icebergs containing substantial englacial debris content are likely to transport ice-rafted debris (IRD) over long distances.

Glacial history and sediment transport

During the last glacial maximum (LGM) there was a continuous girdle of ice around Baffin Bay. On the WG side, ice probably extended to the shelf break (O'Cofaigh et al. 2010; Weidick and Bennike 2007), whereas its position on the BI side is less certain but certainly extended at least to the fiord mouths (Briner et al. 2003, 2007). To the north, the Innuitian and Greenland ice sheets were fused across Smith Sound – Nares Strait (Blake 1975; England 1999; Dyke et al. 2002). Major ice streams were directed to Baffin Bay from all the surrounding ice sheets (Fig. 1; De Angelis and Kleman 2007), including a carbonate-bearing ice stream in Home Bay (Andrews et al. 1970; Tippett 1985; Fig. 1, HB) and with large ice streams in the major structural troughs of Lancaster and Jones sounds (Marshall et al. 1996). Deglaciation was underway by 13–15 cal ka with a major detrital carbonate unit dating from ~12–13 cal ka BP. The channels between NW Greenland and Ellesmere Island were not

Table 1. ^{14}C dates and sediment accumulation rates (SARs) in Baffin Bay.

Late Quaternary dates						
Core ID No.	Latitude	Longitude	Water depth (m)	Depth in core (m)	^{14}C date	Average SAR (cm/ka)
HU77029-006	73°12.1′	67°49.42′	2200	26	12 945±110	1.8
HU26029-025	69°12.3′	62°25.5′	1910	73.5	12 830±95	5.1
HU76029-040	70° 42.4′	64°5.7′	2041	75	13 170±125	4.8
HU77029-017	66°54.09′	58°17.71′	935	127	11 830±90	9.6
HU77029-017	66°54.09′	58°17.71′	935	53	10 800±50	4.4
HU76029-034	71°46.1′	64°22.2′	2275	36.5	12 370±105	2.6
HU74026-557	67°29.8′	60°00.7′	1636	174	12 680±125	12.3

Fig. 2. Paleozoic carbonate and early Tertiary volcanic (Tv) outcrop map; Sea ice extent showing the 30 year median coverage for July 9th; major tidewater and iceberg sources (Bigg, 1999), surface currents, and Arctic Ocean sea ice coverage.

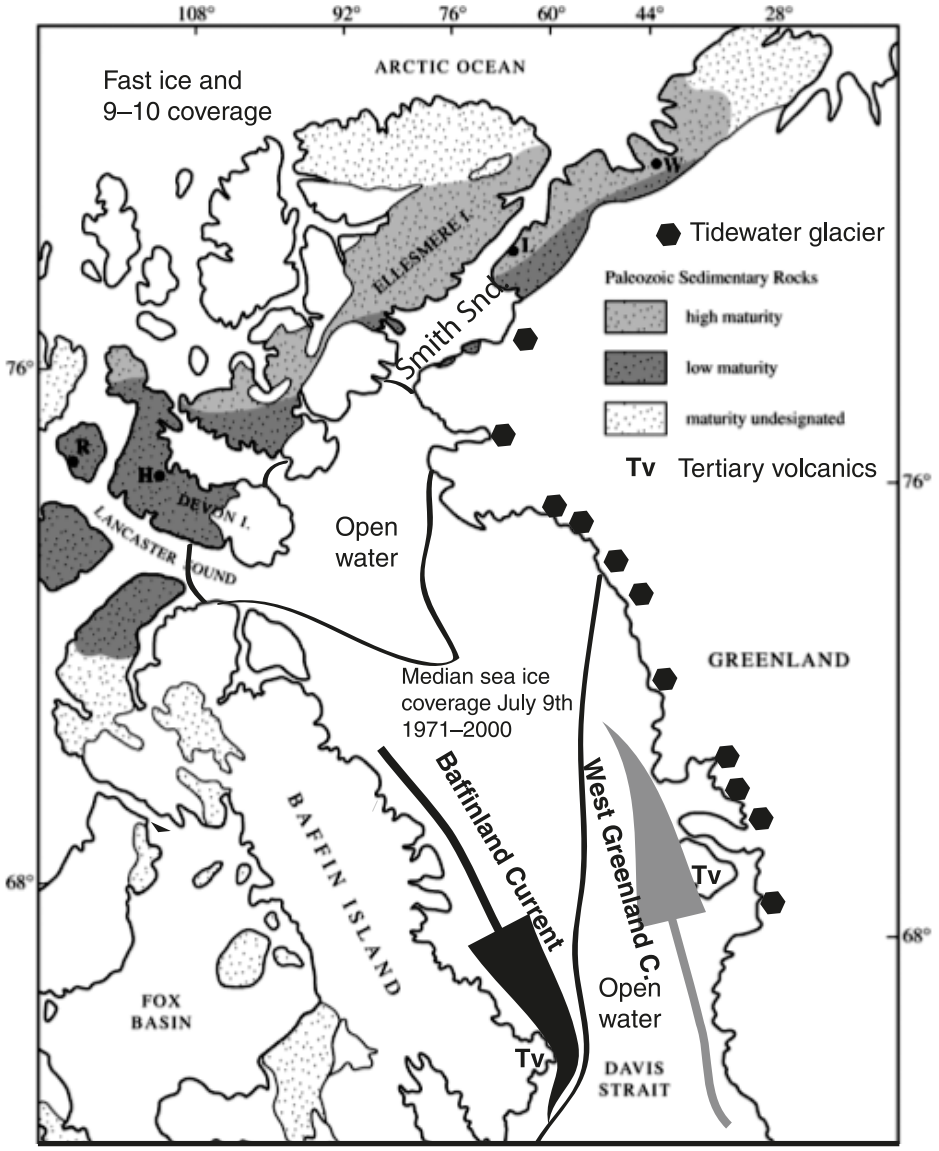

deglaciated until 8.5–8.6 cal ka BP. (Dyke 2004). The GIS retreated behind its present margin ~6 cal ka BP and readvanced during the Neoglaciation, as did glaciers and ice sheets on the Canadian Arctic islands (Davis 1985; Weidick and Bennike 2007).

The fiords of BI and WG have thick Holocene sediment fills; sediment accumulation rates (SARs in cm/a) decline seaward and are low within Baffin Bay itself (Gilbert 1985; Syvitski 1989; Andrews 1990; Syvitski and Hein 1991; Gilbert et al. 1998; Praeg et al. 2006). Sediment-rich meltwater

plumes are clearly visible on various forms of imagery and rainout from these plumes, plus that from subsurface hyperpycnal flows, are responsible for the bulk of sediment delivery. However, the rainout of sediments in meltwater plumes tends to decrease exponentially with distance away from a glacier's margin with a half-distance of a few tens of kilometres (Syvitski et al. 1996*a*, 1998). Furthermore, during the Holocene, most turbidity currents likely were limited to the fiords (Syvitski and Hein 1991). Icebergs carry sediments in a variety of grain sizes, but they are also important agents in sediment reworking. The shelves of Baffin Bay are scoured by icebergs (Praeg et al. 2006; Syvitski et al. 1996*b*). Although there are no quantitative observations, it seems reasonable that the scouring will cause resuspension of fine-grained particles.

Estimates of Holocene SARs in Baffin Bay has proven difficult because corrosive waters have prevented the preservation of foraminifera (Aksu 1983; Osterman and Nelson 1989; Jennings 1993); hence, remarkably few dates are available on late Holocene SARs. The few available dates, usually on the glacial–deglacial transition (Andrews et al. 1998; Smith and Licht 2000; Table 1), suggest low SARs, especially considering the glacierized state of the land around Baffin Bay. These dates (Table 1) reflect average SARs over the interval with the assumptions that (*i*) the core top dates from ca. A.D. 1950–2000, and (*ii*) all sediment was recovered. Thus, these estimates are minimum estimates, but they still reflect an overall slow rate of sediment accumulation.

Samples and methods

Surface samples were mainly obtained from the Core Repository of the Geological Survey of Canada, Dartmouth, Nova Scotia, from *CSS Hudson* cruises in 1964, 1977, 1980, and 1983 (Appendix A; Fig. 1). Grab samples were also obtained from cruises HU2008029 and JR175 to Baffin Bay in 2008 and 2009, respectively (Campbell and de Vernal 2009; O'Cofaigh and Party 2009). Box cores were collected on the HU2008029 and JR175 cruises (Fig. 1). The spatial coverage is reasonable although with a concentration of samples from the northern sector of the bay. The samples were freeze-dried prior to undertaking the various measurements outlined in the following sections.

Grain size

Sediment grain size for Baffin Bay sediments were initially described by Trask (1932) and later by Marlowe (1966), Hume (1972), Kravitz (1976), and Aksu (1981). Grain size on the <2 mm sediment fraction was determined on a Malvern laser system (Andrews et al. 2002; McCave et al. 2006).

Magnetic measurements

Dried samples were measured on a Bartington MS2 m with a 10 cm^3 pot; these measurements were then adjusted for sediment density to obtain mass magnetic susceptibility (Walden et al. 1999). Saturated isothermal remanent magnetism (SIRM) and backfield isothermal remanent magnetism (BIRM) were obtained from dried samples, packed firmly into 8 cm^3 paleomagnetic holders and processed in a Molspin Ltd instrument (Walden et al. 1999). The samples were subject to a 1 T field for SIRM with backfields of 0.1 and 0.3 T (Walden 1999). The readings were adjusted to account for the volume and weight of the sediment.

Colour reflectance

The colour of dried sediment was measured using a Colortron™ spectrophotometer (Andrews and Freeman 1996). This measurement is now routine for on-board measurements on opened marine cores (Helmke et al. 2002), using different spectrophotometer makes. The instrument measures reflectance wavelengths between 390 and 700 nm but also reports the information in the CIE international colour designations, where L* measures black to white, a* is blue to red, and b* is green to yellow.

Quantitative X-ray diffraction

The clay- and silt-size mineralogy of Baffin Bay sediments has been described by X-ray diffraction (XRD) methods in several previous studies (Piper and Slatt 1977; Aksu 1981; Andrews et al. 1989*a*; Thiebault et al. 1989; Andrews 1993). In this paper, quantitative (wt.%) data (qXRD) were determined on <2 mm marine sediment fraction using the method described by Eberl (2003, 2004), involving the addition of zincite, and used extensively on Iceland and East Greenland Holocene marine sediments (Andrews et al. 2006, 2010). This method was ranked 3rd in two Reynold Cup competitions, wherein laboratories analyse the composition of "unknown" sediment mixtures (McCarty 2002). The samples were measured on a Siemens D5000 XRD unit between 5 and 65 2-theta at a 0.02 2-theta step with a 2 s count, resulting in 3000 data points. The counts were then imported into the Excel macro program RockJock v.6 (Eberl 2003), with 124 standard patterns, and the degree-of-fit (DOF = minimum absolute difference) between a calculated and an observed pattern calculated. The errors obtained from running replicate standards are usually within the range of ± 1 wt.%. For this study the wt.% of 21 non-clay and 10 clay mineral species was calculated (Table 2). Runs of artificially created mixtures of four minerals against this list resulted in no false positive identifications.

Data treatment

This paper focuses on the qXRD data with two primary goals: (1) to see if there are any distinct spatial and temporal patterns in the measured variables; and (2) to ascertain whether there are statistically significant relationships between, for example, mineral composition and grain size. The data have been analyzed using the programs "Aabel™" and MVSP (Kovach Computing Services 1998), which allow for both spatial mapping and methods, such as principal component analysis (PCA) (Davis 1986). The qXRD data are expressed as a wt.%, with the sum normalized to 100, hence the wt.% constitute a "closed array" (Aitchison 1986, 1999), which can lead to problems in statistical analysis because if the wt.% of one mineral increases then, by definition, the wt.% in one or more species must decrease. The magnitude of this problem decreases as the number of species increases, but we follow Aitchison 1986) and apply a log-ratio transform to the wt.% data. Although qXRD, grain-size, and massMS analyses were carried out on 82 samples, only 60 samples underwent the full suite of measurements.

Table 2. List on non-clay and clay minerals.

Non-clays	Clay minerals
Quartz	Kaolinite (dry branch)
Ordered microcline feldspar	Saponite
Intermediate microcline feldspar	Ferruginous smectite
Orthoclase feldspar	1Md illite (+ dioct mica and smectite)
Anorthoclase feldspar	1M Illite (R > 2; 88% I)
Albite feldspar (Cleavelandite)	1M illite (R > 1, 70%–80% I)
Oligoclase feldspar (Norway)	Biotite (1M)
Labradorite feldspar	Fe-chlorite (Tusc)
Bytownite feldspar	Muscovite (2M1)
Anorthite feldspar	Illite (1M, PD3B)
Calcite	
Dolomite	
Fe-dolomite	
Siderite	
Halite	
Amphibole (ferrotschermakite)	
Pyroxene (diopside)	
Pyrite	
Magnetite	
Hematite	
Maghemite	
Diatoms	
Chert (8.4 nm)	

Fig. 3. Box plot of non-clay and clay qXRD wt.% for all surface samples. The box encloses 50% of the distribution and the horizontal line within the box is the median.

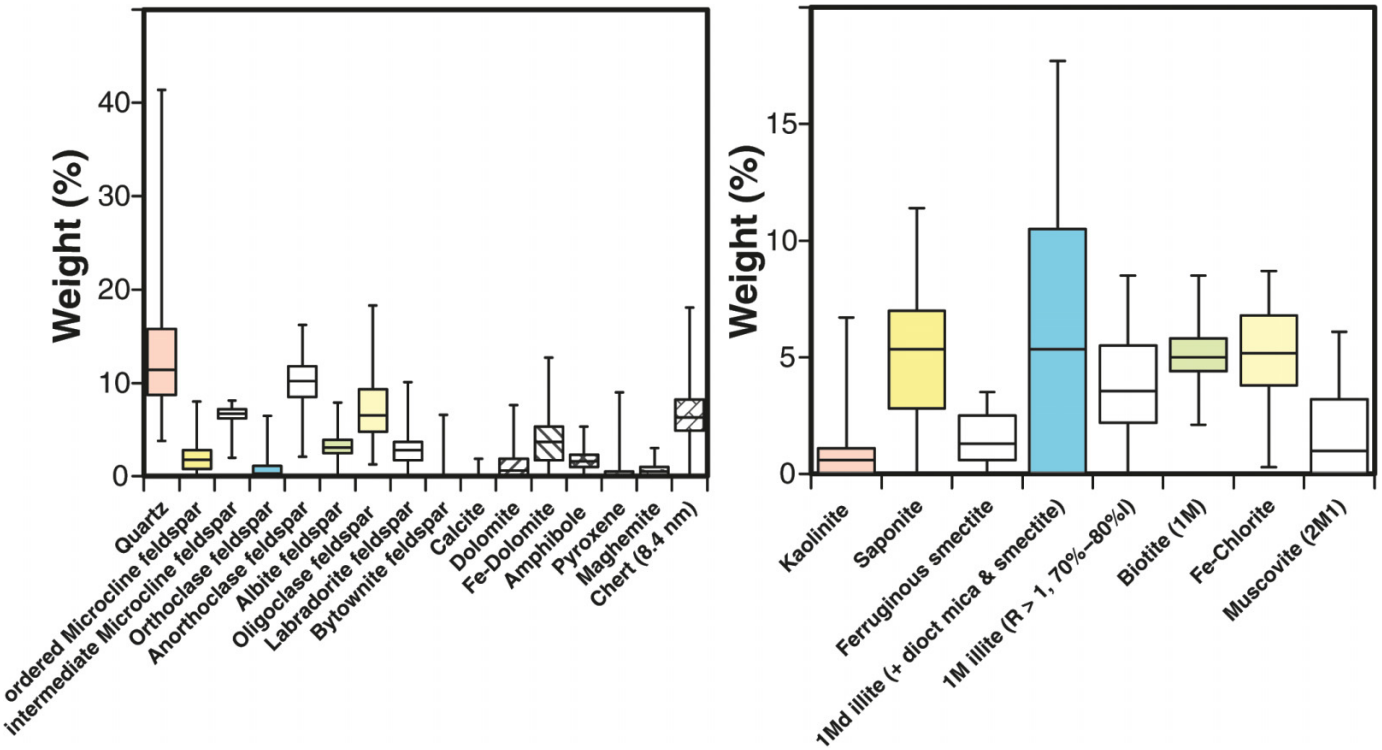

Results — 1. Seafloor mineralogy

Box plots of the 82 samples indicate that the most abundant non-clay minerals are quartz and a variety of K-, Na-, and Ca-feldspars (Fig. 3), with lower amounts of iron-rich dolomite, dolomite, and chert. Calcite is virtually absent (<1 wt.%) in the surface sediments. The clay minerals constitute on average 30 ± 9 wt.% of the surface samples. In terms of weathering products, kaolinite is present but is generally <2 wt.%. There are a variety of smectites, plus ca. 5 wt.% each for 1M illite, biotite (1M), chlorite, and muscovite.

Fig. 4. Contour maps based on the seafloor samples (Fig. 1) of the wt.% of (A) total dolomite, (B) labradorite feldspar, (C) scores on the 1st principal component, and (D) scores on the 2nd principal component (Table 3).

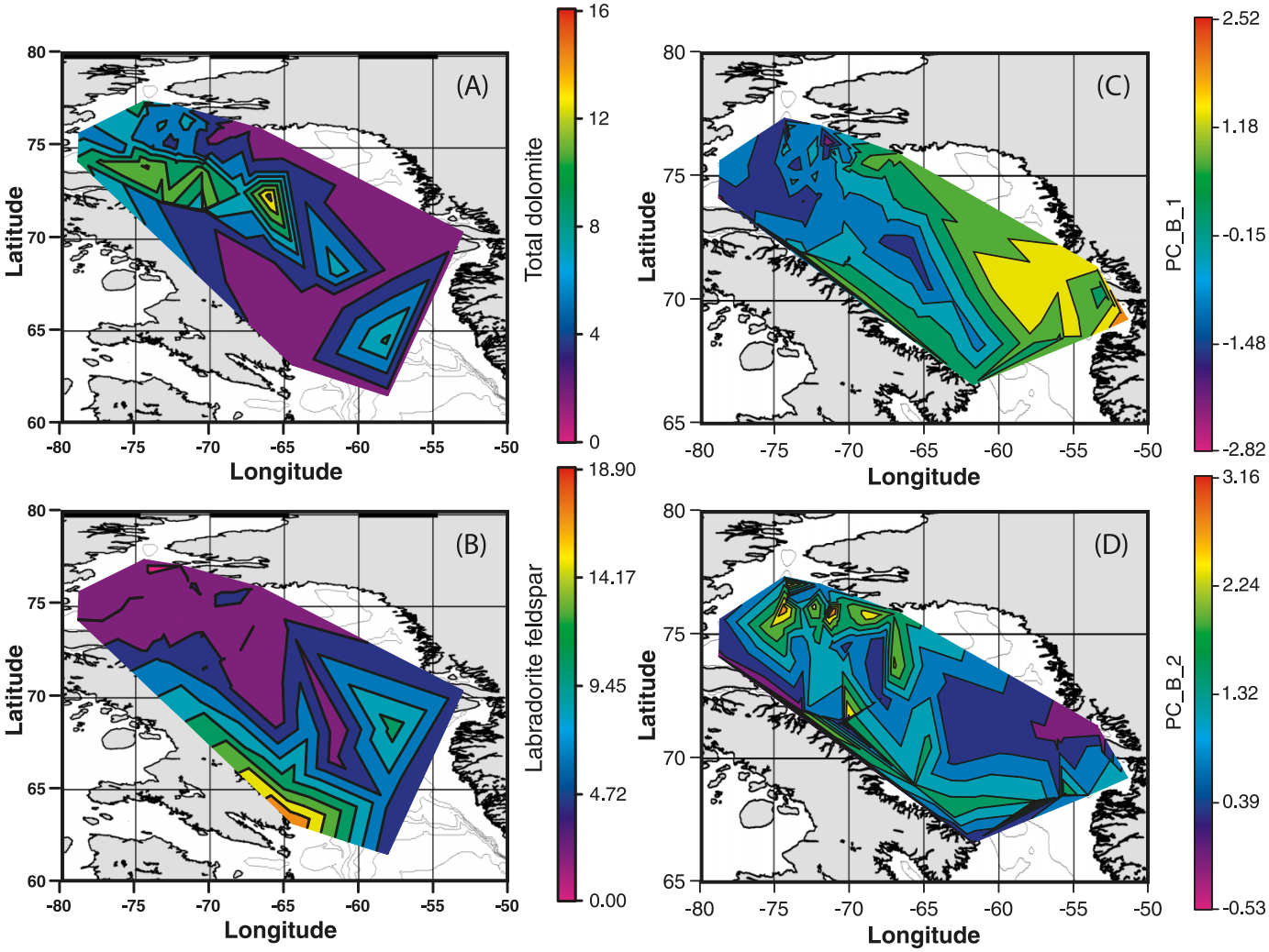

Contour maps of the various mineral species were produced; two of the most interesting distributions are shown in Figs. 4A and 4B. These show a plume of dolomite-rich surface sediments extending from northern Baffin Bay along the elongated axis of the bay (Fig. 4A); in contrast, the distribution of labradorite is concentrated in the southeast section of the bay in areas near the early Tertiary volcanic outcrops but extending northward along the west side of Baffin Bay (Fig. 4B).

To gain a better understanding of the mineral composition of the surface sediments, principal component analysis of the transformed log ratio wt.% data was undertaken (Aitchison 1986; Davis 1986). Species that contributed <2 wt.% were excluded; thus, initially 23 minerals were included in the PCA. The 1st three axes explain, cumulatively, 20%, 31% and 42% of the total variance, but several minerals had low loadings on the axes. After excluding five minerals that had loadings <0.2 on one of the 1st three PC axes, the variance explained increased to 22%, 36%, and 49% (Table 3). The 1st axis is positively associated with amphibole and several feldspars, and negatively associated with dolomite; the 2nd axis is strongly linked with quartz (+) and saponite (–). Contour maps of the 1st two PC scores (Figs. 4C, 4D) indicate a geographical clustering; scores on the 1st PC show a broad belt of negative scores in northern Baffin Bay with a long, narrow extension of negative scores (dolomite) running along the deep axis of the bay (Fig. 4D). The scores on the 2nd PC are dominated by a broad area of negative scores in SE Baffin Bay extending seaward from the general area of Disko Bugt.

Given the dominance of Precambrian igneous and metamorphic rocks in the surface outcrop surrounding Baffin Bay, a logical null hypothesis is that there are no significant site differences in the non-clay and clay mineral abundances. However, minimum variance cluster analysis (Kovach Computing Services 1998) of the PC scores on the 1st three axes indicated two or three major clusters of sites based on their composite mineralogy (Fig. 5). Geographically, they represent somewhat discrete areas within Baffin Bay, although there is some overlap (Figs. 4C, 4D).

Discriminant function analysis (DFA; Davis 1986) can be used to test the research hypothesis that the clusters (Fig. 5) represent distinct groupings, versus the null hypothesis that the clusters are not distinct from each other. Using 14 non-

Table 3. Principal component analysis (PCA) data.

Loadings on logratio transform	PC_1	PC_2	PC-3	PC1	PC2
Eigenvalues	4.11	2.72	2.49		
Varience (%)	21.61	14.34	13.08		
Variance (cumulative %)	21.61	35.95	49.03		
—				r2	r2
Quartz	0.11	0.47	0.05	0.07	0.55
Ordered microcline feldspar	0.32	0.07	0.06	0.61	0.02
Intermediate microcline feldspar	–0.37	0.19	0.19	–0.49	0.02
Anorthoclase feldspar	–0.1	0.16	0.36	0.002	0
Oligoclase feldspar	0.4	0.12	–0.01	0.72	0
Labradorite feldspar	0.36	0.02	0.2	0.67	0
Total dolomite	–0.34	0.07	0.24	–0.36	0
Amphibole	0.32	–0.05	0.02	0.51	
Pyroxene	0.16	0.02	–0.24	0.16	
Maghemite	0.05	–0.28	0.01	0.016	0.2
Chert (8.4 nm)	–0.04	0.29	0.25	0	
Saponite	–0.1	–0.46	–0.13	–0.01	–0.68
Ferruginous smectite	–0.09	–0.21	0.12	–0.09	
mica and smectite	–0.1	0.19	–0.46	–0.15	
1M Illite (R > 2; 88% I)	–0.11	0.23	–0.15	–0.06	
1M illite (R > 1, 70%–80% I)	–0.06	–0.19	0.46	–0.03	–0.2
Biotite (1M)	0.06	–0.25	0.25	0.03	–0.23
Fe-chlorite	–0.33	–0.17	–0.26	–0.42	
Muscovite (2M1)	–0.21	0.24	–0.02	–0.47	

Fig. 5. Cluster of surface sites based on the PC scores — minimum variance and Euclidean distance squared are the clustering criterion (Kovach, 1998). Three clusters A, B, and C are identified (see text and Fig. 6A). The capital letters to the right (U, J, EB, and NB) refer to Umanak and Jakobshavn troughs, and East and North Baffin Bay, respectively (see Fig. 6 and text).

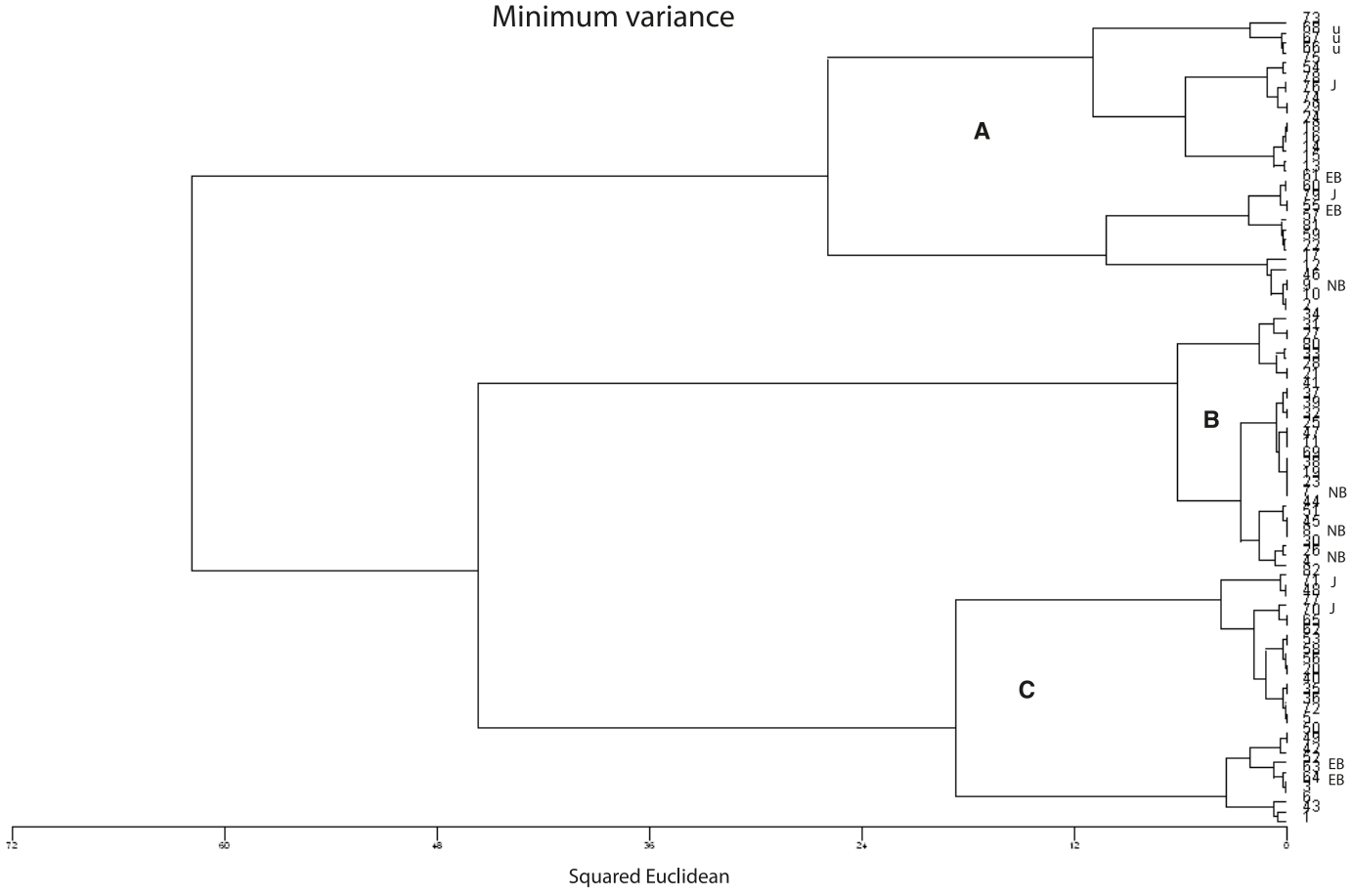

Fig. 6. (A) Scatter plot of the 1st two discriminant function analysis (DFA) scores of the three principal component analysis clusters. (B) Box plot of the wt.% of the main discriminating minerals in each of the three clusters (Fig. 5). (C) Discriminant function scores of the proposed four end-member compositions (Fig. 5) that are applied to the unmixing of JR175BC06, including quartz but excluding carbonate (see text and Figs. 10 and 11). Shaded area represents overlap between East Baffin and Jakobshavn Trough (J) sites (see also Fig. 5). U, Umanak Trough.

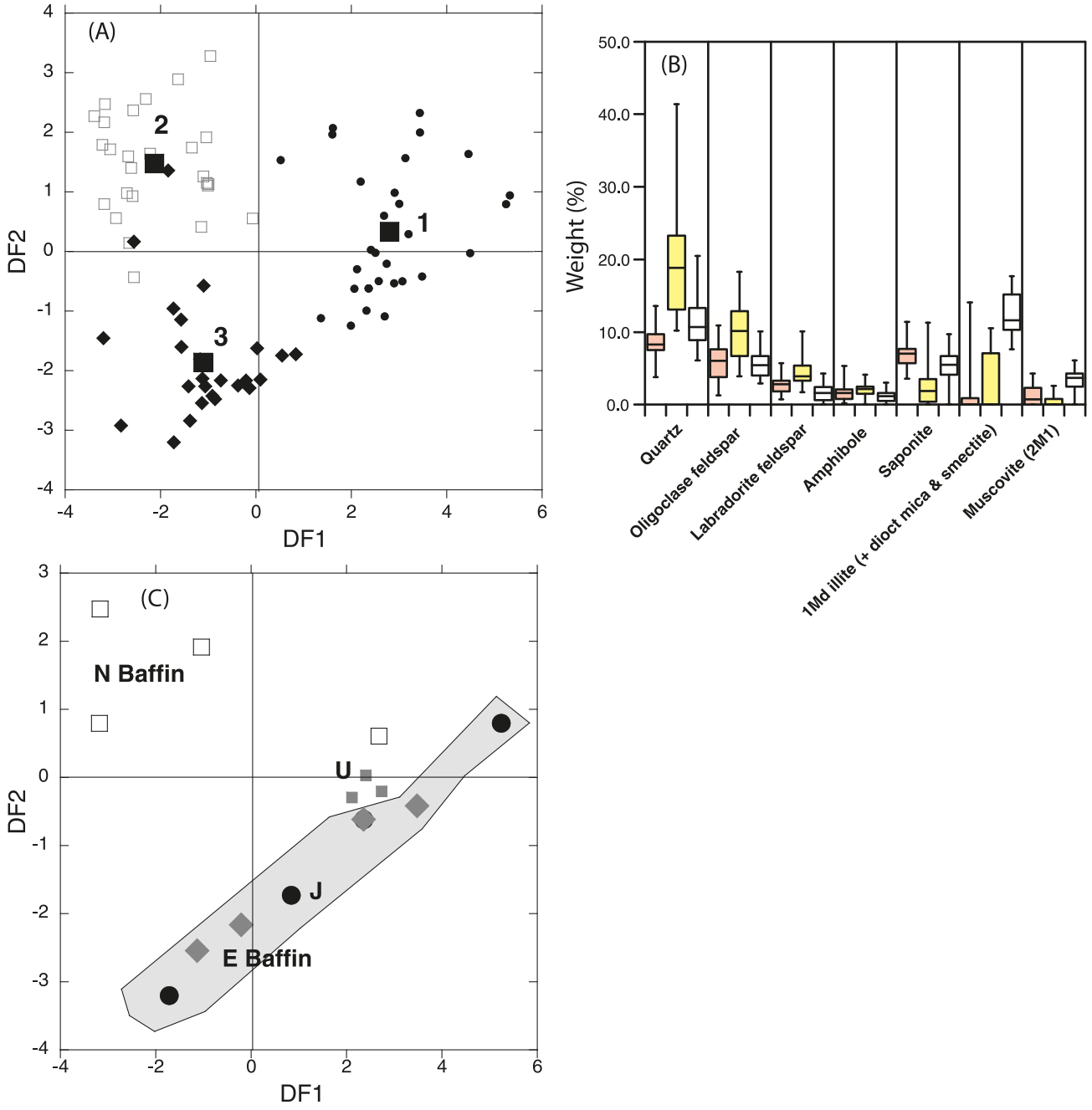

clay and clay mineral species the classification of three clusters is 97% correct (three misclassified; Fig. 6A). If only the non-clay minerals are used, then 11 samples (13%) are incorrectly classified — the misclassifications only affected groups B and C, which were part of a larger grouping (Fig. 5). Two samples from the deepest part of the bay (HU77-17 and HU77-18) were repeatedly classified in group B, not group C. Stepwise DFA indicates that the variables that best discriminate between the clusters are illite–smectite, quartz, oligoclase feldspar, saponite, muscovite, labradorite, and amphibole (Fig. 6B), dolomite was not chosen in the stepwise procedure. Combining clusters B and C (Fig. 5) and using DFA resulted in only one sample misclassification.

An important question is how far the mineralogical differences are associated with other sediment properties, such as grain size, magnetic characteristics, and colour? Correlation of the 1st PC scores against sediment properties indicated highly significant correlations ($p < 0.001$) with magnetic characteristics and grain size (Figs. 7A–7C) but not with any of the CIE* colour properties (Fig. 7D). Indeed, further in-

Fig. 7. (A–F) Correlations between PC-1 scores and various sediment properties. The least squares regression equations, values of r^2, and probability (p) of the null hypothesis (no correlation) being correct are shown at the top of each graph. (A) Mass magnetic susceptibility; (B) Phi Mean; (C) backfield isothermal remanent magnetization (BIRM); (D) "red" colour (a*); (E) quartz wt.% versus sand %; (F) clay (grain size) versus total clay wt.% from qXRD.

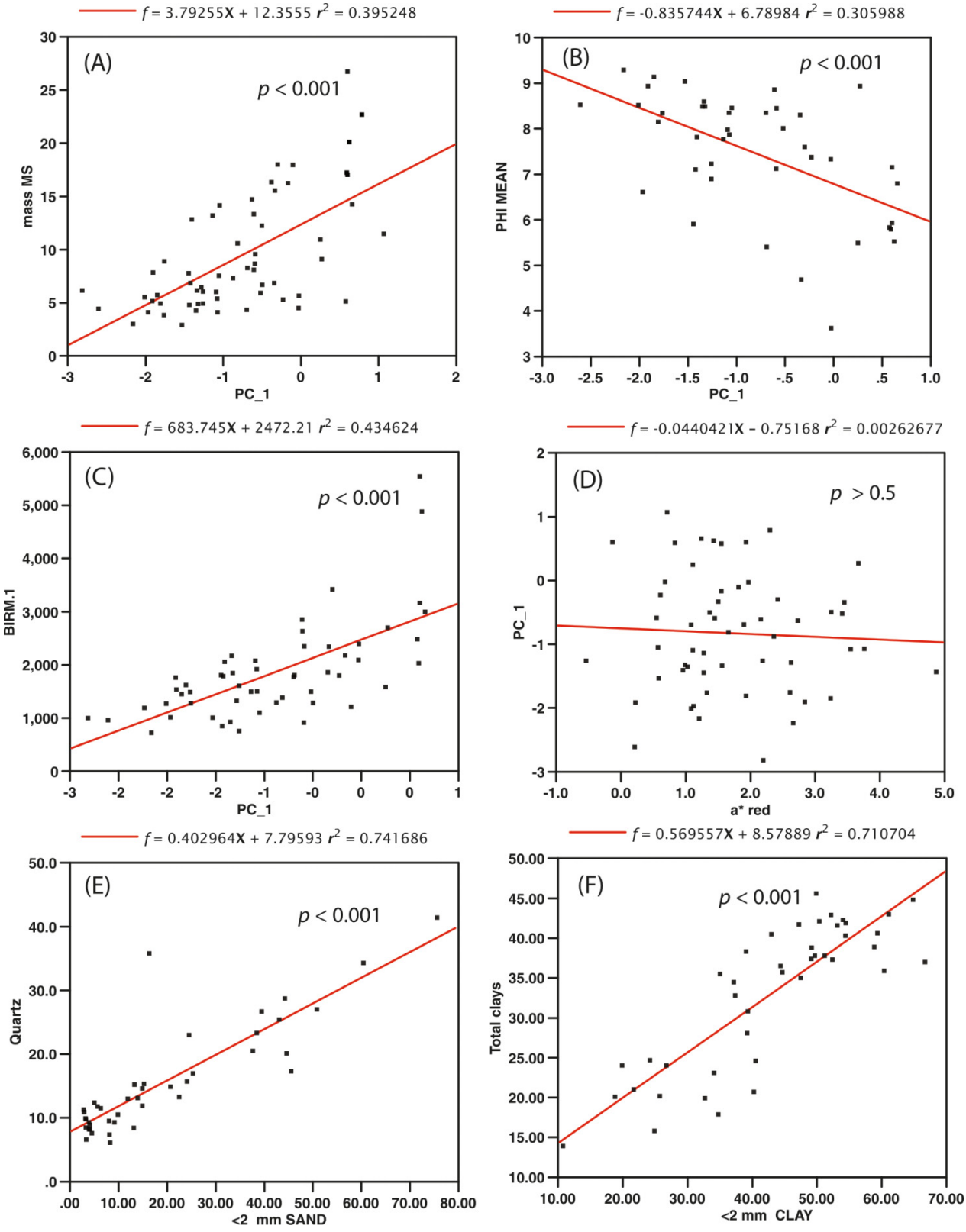

Fig. 8. Weight % of calcite (= cal) and dolomite (lines with solid squares) plotted against depth for six box core. wd, water depth (in m). JCR175BC01 was omitted, but it has the same very low levels of calcite as the nearby box core HU2008029-068BX. Note the different values for the *y* axes between the shallow versus deep core sites.

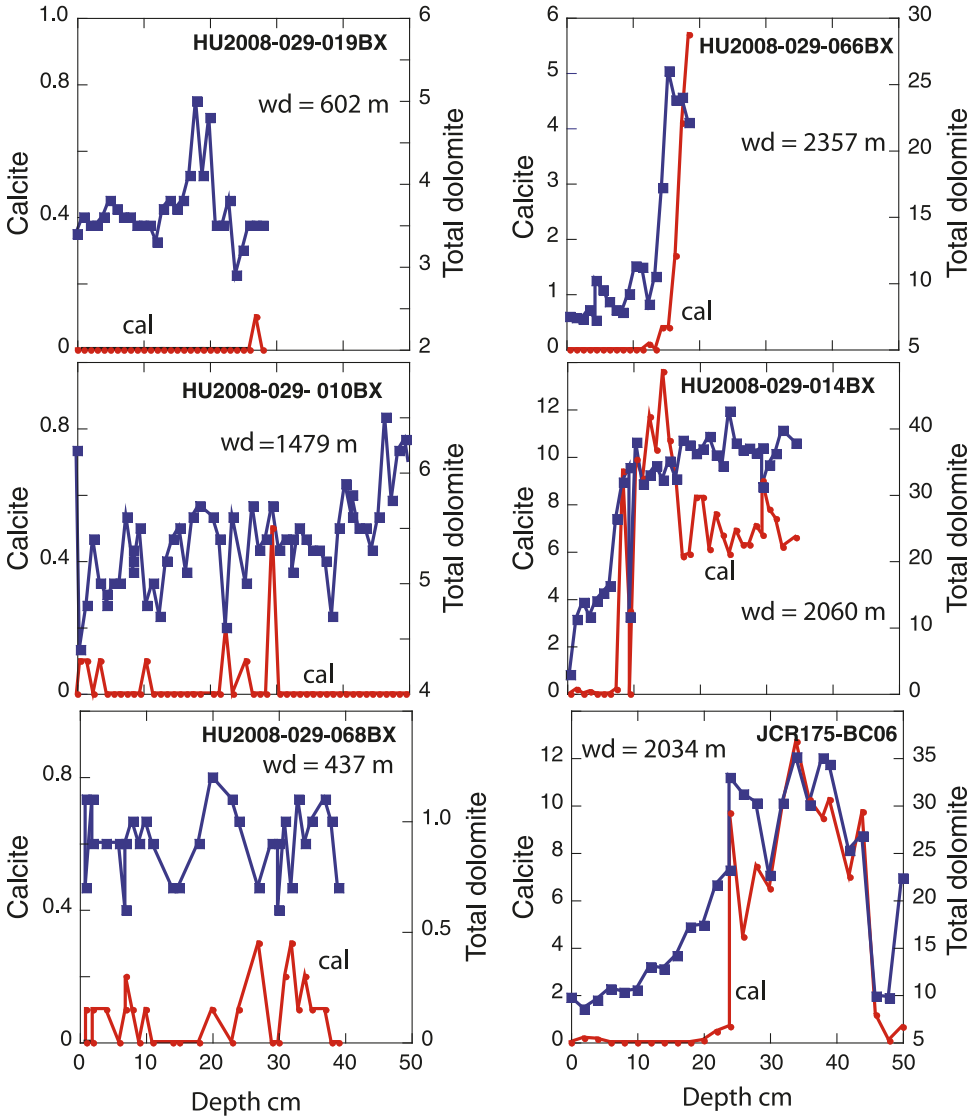

vestigation indicates that ~75% of the variance in the quartz wt.% is associated with the wt.% sand (Fig. 7E). Similarly, the fraction of sediment in the clay-size fraction (<2 μm) is strongly correlated with the wt.% of the clay mineral fraction (Fig. 7F). Water depth (not shown) is associated with % clay (grain size) and with the wt.% clay minerals (r^2 = 0.26 and 0.16, respectively). Dry sediment "redness" colour values were positively associated with water depth (r^2 = 0.4), such that "redness" had values of a* ≥ 3 (i.e., "red") at depths >2000 m (Fig. 7D). Fifty-four percent of the variance in sediment colour was explained by a combination of water depth and clay-size percent.

Results — 2. Box cores: calcite and dolomite

The future application of the surface mineralogy to down core mineral provenance variations is a primary rationale for the qXRD of surface sediments (Andrews et al. 2010). Several box cores from HU2008029 and JCR175 were analyzed (Fig. 1; Appendix A) — there are presently no radiocarbon dates on the box cores. The selected cores are aligned along the axis of the bay and, thus, tend to be located along the trajectory of the main dolomite plume (Fig. 4A). A striking feature of three box cores from the deep central basin (Fig. 8) is the very low abundance of calcite, with values ~0 wt.% in the uppermost few centimetres compared with calcite wt.% estimates of 5%–12% deeper in the cores (Fig. 8). Virtually no calcite was detected in the surface samples nor in HU2008029-10BC, HU2008029-019BC, HU2008029-068BC nor JCR17501BC (i.e., Azetsu-Scott et al. 2010). The total dolomite wt.% can reach nearly 40 wt.% deeper in the cores, but it also shows a strong decrease to ~10 wt.% coincident with the disappearance of calcite in the upper sections of the cores (Fig. 8). During the peak detrital carbonate interval, the ratio of calcite:dolomite is of the order of 0.23:1 and, thus, contrasts markedly with the ratio off Hudson Strait (Fig. 1), where the ratio is around 6:1 during Heinrich (H-) events (Andrews and Tedesco 1992). Repeated evidence for

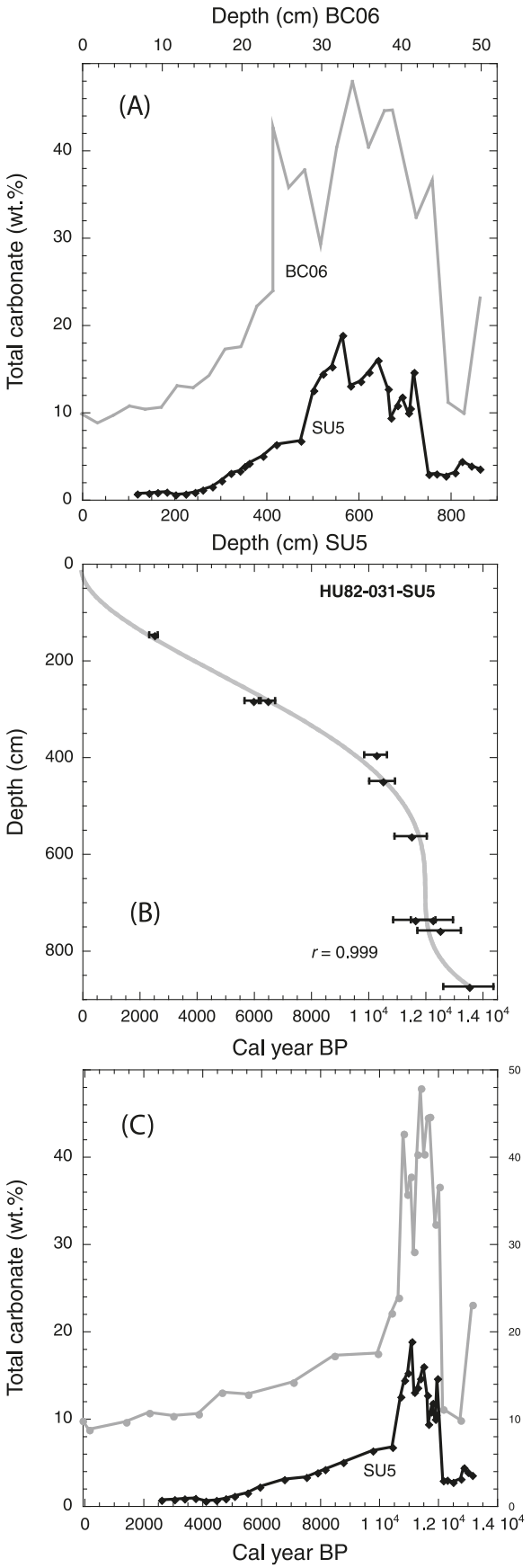

Fig. 9. (A) Overlay of SU5 and JCR175BC06 on total carbonate/dolomite. (B) Depth/age plot for HU82-031-SU5PC. (C) Proposed age model for the JR175BC06 box core.

Holocene calcite dissolution in Baffin Bay and the Labrador Sea has been reported (Aksu 1983; Osterman and Nelson 1989; de Vernal et al. 1992; Knudsen et al. 2008), although fixing an age has been difficult. In cores from northern Baffin Bay (HU2008029-034PC) and NW Labrador Sea (HU90-023-022PC) (Fig. 1) unpublished qXRD data indicate that calcite reaches ~0 wt.% around 5 cal ka BP. If this age is applied to the deep basin box cores then sediment accumulation rates of between 1.6 and 4 cm/ka apply (compare with Table 1). At the ODP site 645 (Srivastava et al. 1987, p. 144), the research suggested that there have been repeated cycles of calcite dissolution coinciding with "…..warm 'interglacial' periods…"

We next compare the carbonate record from HU82031-SU5 (SU5) — a piston and Lehigh gravity core taken in Sunneshine Fiord (Syvitski and Blakeney 1983; Andrews et al. 1996), which is located in the southwest sector of Baffin Bay (Fig. 1), with that from JCR175BC06 (BC06) (Figs. 1, 9). Kranck (1966) reported present day carbonate-bearing icebergs in the area of Sunshine Fiord. SU5 has 11 accelerator mass spectrometry (AMS) ^{14}C dates on foraminifera or mollusks, ranging in age between ~3 and 12 ka BP (Andrews et al. 1989*b*). Calibration of the dates and interpolation of a depth/age model (Fig. 9B) was accomplished using OxCal with the marine Intercal 98 curve (Ramsey 2008) with a ΔR of 50 ± 50 years. A somewhat larger ΔR may indeed be appropriate, but at the moment, we lack data on the variability of the ΔR in Baffin Bay over the last 12–13 cal ka BP. The basal calibrated age is 13 550 ± 65 cal years BP and the peak in DC was linked to a Younger Dryas interval both on the basis of the ages and a dramatic increase in a species of Arctic benthic foraminifera (Andrews et al. 1996). The records from SU5 and BC06 can be correlated ($r = 0.91$) with only five tie points in AnalySeries (Paillard et al. 1996); the depth/depth correlation was then used to develop a depth/age plot for BC06 (Fig. 9C). The average SAR for BC06 is ~4 cm/ka; thus, similar to the rates noted in Table 1. The derived chronology for BC06 should be considered as a working hypothesis that requires verification from AMS radiocarbon dates and (or) other correlation tools. AMS radiocarbon dates from the uppermost 20 cm will be nearly impossible to obtain because of calcite dissolution. However, the main point of Fig. 9 is to draw attention to the possibility of robust correlations in Baffin Bay based on changes in sediment mineralogy.

Results — 3. Changes in sediment sources

A critical question in terms of down core mineralogy is — can we infer any changes in sediment provenance? This question requires that we attempt to "unmix" the sediment mineral compositions relative to defined end members (i.e., sources). We use the Excel Solver macro program "AutoMinUnMix v.3" (AMUMv3; Eberl 2004; Andrews et al. 2010; Appendix B) to estimate changes in composition. A DOF statistic (Eberl 2004) and the average absolute wt.% deviation for each composition are calculated (e.g., Fig. 10), as is the

Fig. 10. Representative plots (A, B, C) of examples of observed (open) and estimated (gray) wt.% compositions for down core sediments in JCR175BC06 based on normalized data excluding carbonates and quartz — note that the *y* axis scales are not the same. Each comparison shows depth and estimated age, sum of the four estimated compositions, degree-of-fit (DOF), and the average departure or deviation of observed and estimated wt.% (see Appendix B).

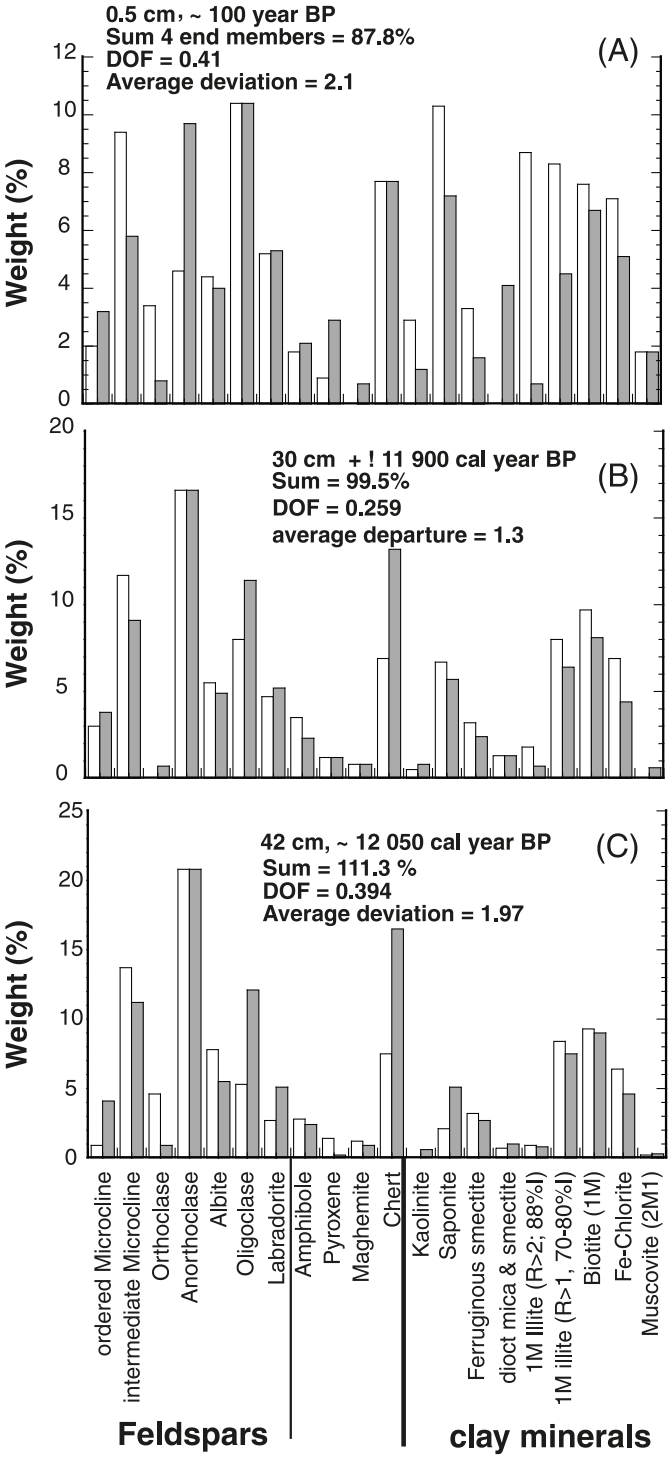

estimated total wt.% (Appendix B). Ideally this should sum to 100%, but in practice, the sum will vary (Figs. 10, 11A).

The first question is does the down core compositions differ from the surface sediments? To address this question, we used AMUM and calculated the "similarity" between the surface (0–1 cm) and down core compositions in BC06 using 31 mineral species; thus, values close to 100 wt.% represent similar compositions to the surface mineralogy, whereas much lower values indicate different compositions. Thus, down core compositions are rather similar to the surface mineralogy between 0 and 20 cm, and also around 32 and 45 cm, but very different compositions occurred between 20–30 and 30–45 cm depth (Fig. 11A).

Fig. 11. Data for JR175BC06 plotted against depth (in cm) — age estimates (sold vertical black lines) of the carbonate peak based on Fig. 9C. (A) Sum wt.% of a comparison between the mineralogy from 0 cm and the down core samples. Large deviations from 100% indicate major changes in mineral composition. (B) Average wt.% species deviations for each sample of JT175BC06 based on four sources and excluding carbonate and quartz. (C) Cumulative wt.% contributions from the four sources and the total wt.% carbonate (gray). "Not resolved" indicates that the sum wt.% was <100.

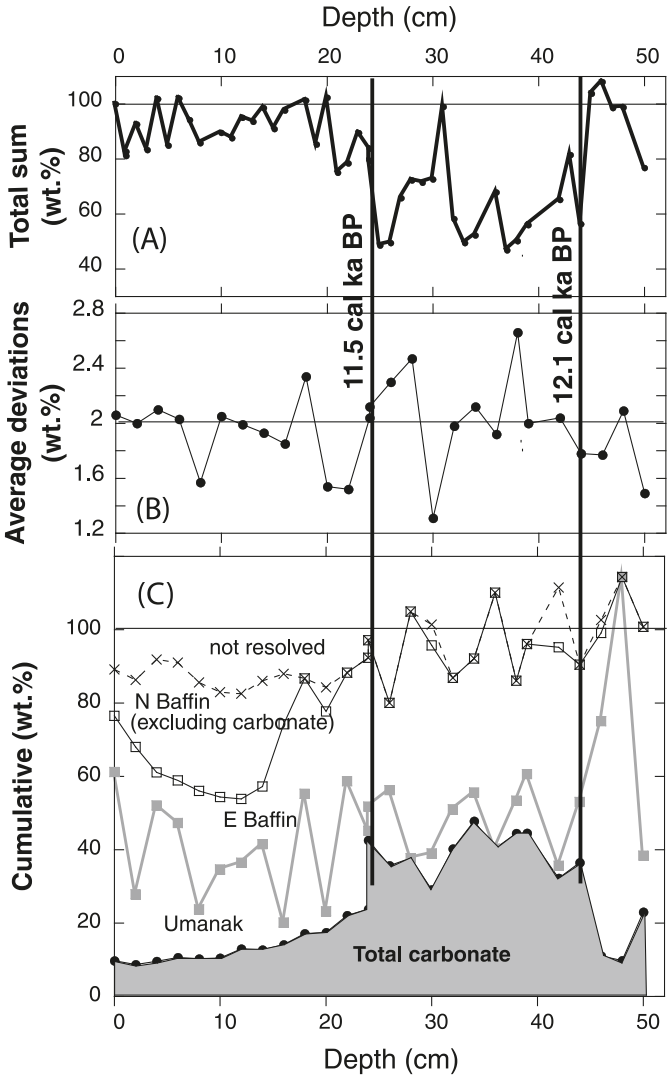

The variations in Fig. 11A indicate major changes in primary sediment sources; hence, the next question is whether we can pinpoint the sources. We use AMUM to allocate changes in sediment provenance archived in BC06. We de-

Table 4. Average wt.% data from four possible source areas.

	Jak	Uman	EB	NB
Quartz	14.5	12.7	14.3	19.9
Ordered microcline feldspar	2.7	4.8	3.2	0.8
Intermediate microcline feldspar	5.7	3.0	8.6	7.3
Orthoclase feldspar	0.5	0.1	0.6	1.6
Anorthoclase feldspar	16.7	5.0	16.2	11.0
Albite feldspar	3.8	4.4	4.2	3.5
Oligoclase feldspar	10.3	14.2	9.5	5.3
Labradorite feldspar	6.7	8.4	4.0	1.3
Amphibole	3.8	2.8	1.9	1.0
Pyroxene	2.6	6.4	0.1	0.0
Maghemite	1.6	0.5	0.7	0.9
Chert (8.4 nm)	6.4	5.1	12.6	7.4
Kaolinite	2.0	1.9	0.5	0.7
Saponite	5.5	10.9	4.1	4.6
Ferruginous smectite	1.4	2.0	2.3	1.0
1Md illite (+ dioct mica and smectite)	0.0	0.1	0.1	12.1
1M Illite (R > 2; 88% I)	0.1	0.7	0.7	0.5
1M illite (R > 1, 70%–80% I)	5.3	4.1	5.9	4.2
Biotite (1M)	6.4	7.5	7.0	5.2
Fe-chlorite	3.8	4.5	3.4	7.1
Muscovite	0.0	0.9	0.0	4.5
Total	100.0	100.0	100.0	100.0
Ordered microcline feldspar	3.2	5.5	3.8	1.0
Intermediate microcline feldspar	6.7	3.5	10.1	9.2
Orthoclase feldspar	0.6	0.1	0.7	2.0
Anorthoclase feldspar	19.6	5.7	18.9	13.7
Albite feldspar	4.4	5.0	4.9	4.4
Oligoclase feldspar	12.1	16.3	11.1	6.6
Labradorite feldspar	7.8	9.7	4.6	1.6
Amphibole	4.4	3.2	2.2	1.3
Pyroxene	3.1	7.3	0.1	0.0
Maghemite	1.8	0.6	0.8	1.2
Chert (8.4 nm)	7.4	5.9	14.7	9.2
Kaolinite	2.3	2.2	0.6	0.9
Saponite	6.5	12.5	4.8	5.8
Ferruginous smectite	1.7	2.3	2.6	1.2
1Md illite (+ dioct mica and smectite)	0.0	0.1	0.1	15.1
1M Illite (R > 2; 88% I)	0.2	0.9	0.8	0.6
1M illite (R > 1, 70%–80% I)	6.2	4.6	6.9	5.2
Biotite (1M)	7.5	8.6	8.2	6.5
Fe-chlorite	4.5	5.1	4.0	8.9
Muscovite	0.0	1.0	0.0	5.6
Total	100.0	100.0	100.0	100.0

Note: Jak, Jakobshavn Trough; Uman, Umanak Trough; EB, east Baffin Island; NB, north Baffin Bay.

fine four end members based on likely glacial sources (Figs. 1, 5; Hiscott et al. 1989; O'Cofaigh et al. 2010), namely (1) north Baffin Bay – Lancaster Sound (LS) and Jones Sound (JS), (2) eastern Baffin Island (SI, HB), (3) Umanak Trough (U), and (4) Jakobshavn Trough (J). In glacial marine environments, there are no truly unique end members; therefore, for each of the potential source regions, we used average wt.% values from four separate surface samples (Table 4). Figure 5 illustrates that the geographic selection of sites does not totally mimic the cluster diagram, although the Umanak Trough sites (cluster A) and the North Baffin sites (cluster B) are reasonably distinct, whereas the Jakobshavn and East Baffin sites range between clusters A and C (Fig. 5). Scores from the DFA (Fig. 6A) are plotted for the selected end members (Fig. 6C). The results indicate that the four end member compositions are discrete, although a case could be made for three end members by combining Jakobshavn and eastern Baffin Island. (Fig. 6C, shaded grey area).

The peak in carbonate content in BC06 (Fig. 11C) indicates a major axial source from northern Baffin Bay, the only caveat is that the contribution of the carbonate-bearing ice stream across Baffin Isand to Home Bay (Fig. 1; Andrews et al. 1970; Tippett 1985) is poorly known. Although at ca. 10 cal ka BP the wt.% dolomite in HU85-079TWC,

outer Home Bay (Fig. 1) is only 8%. The box core mineralogy indicates a significant "no analog" problem since in the surface sediment, calcite is absent because of the corrosive waters (Azetsu-Scott et al. 2010) and the dolomite wt.% is significantly lower than that of the down core peak (Fig. 11C). In Fig. 11A, this problem is expressed as the low sum wt.% between 25 and 45 cm (~11.5 and 12.1 cal ka BP). To circumvent this problem, the wt.% of carbonate species and any mineral with <2 wt.% were removed and compositions re-calculated to sum to 100% (23 species). The subtraction of carbonate effectively reduces the impact of the northern Baffin Bay in our source-attribution calculations. Because of the overall ubiquity of quartz in the compositions (average 13.7 ± 7 wt.%), we also recalculated an additional data set after the removal of quartz (22 species; Table 4).

AMUM was applied to the down core compositions in BC06. Runs with or without quartz were very similar for the Umanak Trough and East Baffin Island sources (r^2 = 0.94 and 0.73), moderately similar (r^2 = 0.33) for the northern Baffin Bay source, and exhibited no correlation with the Jakobshavn end member. We discuss the results based on the non-carbonate and non-quartz data (Figs. 11B, 11C); the data are plotted as cumulative wt.% (Fig. 11C). Average wt.% deviations (see Fig. 10, Appendix B) for BC06 varied between 1.2 and 2.5 wt.% (Fig. 11B). The largest non-carbonate contribution is attributed to East Baffin (averaged 51%), followed by Umanak (27%), northern Baffin Bay (11%), and Jakobshavn (2%). The small contribution from the Jakobshavn Trough is understandable as BC06 lies well north of the trough outlet (Fig. 1). The averages hide substantial variations. The graph indicates that a major contribution from the Umanak Trough occurred immediately prior to the carbonate peak, which is thought to be associated with the Younger Dryas cold event (Andrews et al. 1996).

Conclusions

A study of the qXRD mineralogy in the <2 mm sediment fraction from the present-day seafloor sediments of Baffin Bay (Fig. 1) indicate some spatial clustering among the measured compositions. A plume of dolomite can be detected than runs along the axis of the bay, whereas calcite is not present (Fig. 4A). The scores on the 1st PC axis indicate that the mineralogies are strongly associated with both grain size and magnetic mineral properties (Fig. 7). Cluster analysis on the first three PC axes scores suggests two to three major compositional groupings (Fig. 5); discriminant function analysis indicates that these are statistically distinct with only one misclassifications. These results, plus the compositional unmixing (Fig. 11), indicate that we can partly reject the hypothesis that we cannot differentiate between sources despite the dominance of felsic rocks around much of Baffin Bay.

qXRD analyses of sediments from the lower half of 20–50 cm long box cores indicate the presence of some calcite but much larger amounts of dolomite. These studies re-affirm the critical importance of detrital carbonate-rich (DC-) facies in understanding the deglacial history of the northeastern Laurentide, southern Innuitian and NW Greenland ice sheets. Significant fractions of the beds of these ice sheets, principally in the northern part of the region, eroded Paleozoic carbonates (Fig. 2). The straightforward application of the surface mineralogy to down core interpretation of changes in sediment provenance are hampered by the "no analog" problem associated with the dissolution of calcite. Compositional unmixing of down core mineralogy in BC06, excluding carbonate, indicated variations in sediment sources during the last deglacial–Holocene cycle. The presence of significant amounts of detrital carbonate throughout central and western Baffin Bay during deglaciation requires transport by a combination of iceberg rafting and suspended sediment in meltwater plumes. This transport path is visible today (Fig. 4A). The relative fluxes of detrital carbonate to the deep basin and eastern Baffin Island shelf can be estimated by comparing SU5 and BC06 (Fig. 9). Based on layer thicknesses the DC fluxes at these two core sites differ by an order of magnitude (~250 cm versus 25 cm). Yet if the differing carbonate wt.% are taken into account, the relative fluxes are less disparate, differing only by about a factor of 3. Rough DC flux estimates are 30 mg/cm/a at SU5 versus 11 mg/cm^2/a at BC06, assuming that the two DC events are coeval (Fig. 9C). We interpret this observation to mean that dolomite was being carried southward along the Baffin Island shelf across Davis Strait (Fig. 1), where the plume would merge with the more calcite-rich sediment plumes sourced from Hudson Strait (Hesse et al. 1990; Andrews and MacLean 2003).

The sediment mineralogy does not per se provide information on specific transport or depositional processes, and the mineralogical data needs to be integrated with studies of lithofacies, sediment magnetic properties, and diffuse spectral reflectance of the cores collected during the HU2008029 and JR175 cruises (Kilfeather et al. 2010; Ortiz 2009). The successful integration of a lithofacies and provenance approach will be facilitated by the application of programs like AMUNv.3 (Appendix B; Andrews et al. 2010). Furthermore, the non analog problem noted earlier in the text (Fig. 11) will be circumvented by qXRD down core studies of piston cores and vibracores that extend into ice proximal glacial marine sediments associated with the LGM and deglaciation (e.g., Farmer et al. 2003). Such cores already exist (e.g., Knudsen et al. 2008; Hillaire-Marcel et al. 1989) and additional cores were obtained during the HU2008029 and JR175 expeditions. qXRD study of a suite of long (6–12 m) piston cores is underway.

Acknowledgements

Research on the seafloor samples was initially funded by US National Science Foundation (NSF) ATM-0502515. Data collected from cruises HU2008029 and JR175 was supported by NSF OPP-0713755 to Dr. Anne E. Jennings as principal investigator (PI). The authors would like to thank the scientists and crews on both the HU2008029 and JR175 cruises for the collection of samples, as well as the earlier *CSS Hudson* cruises. Chief scientists on these cruises were Drs Calvin Campbell and Anne de Vernal and Colm O'Cofaigh, respectively. The 2008 expedition to Baffin Bay and Davis Strait was supported by the Canadian Foundation for Climate and Atmospheric Science (CFCAS) through a special allocation to the Polar Climate Stability Network (PCSN). Complementary funding was also obtained from the Natural Sciences and Engineering Research Council of Canada (NSERC). The 2009 cruise JR175 of the RRS James Clark Ross was supported by the UK Natural Environment Research Council

(NERC grants NE/D001951/1 and NE/C506372/1). The paper has benefited from reviews by G. Bigg, A. Kilfeather, K. Refsnider, and D. Barber. Ursula Quillmann is thanked for her efforts in sampling the archived material from the Bedford Institute of Oceanography's Core Repository and Kate Jarrett is thanked for her assistance in obtaining these samples and others obtained in 2009 by JTA. We wish to thank Brian MacLean and another reviewer for their comments and criticisms. Data will be archived at www.ncdc.noaa.gov/paleo/data.html.

References

Aitchison, J. 1986. The statistical analysis of compositional data. Chapman and Hall, London, UK. 416 p.

Aitchison, J. 1999. Logratios and natural laws in compositional data analysis. Mathematical Geology, **31**(5): 563–580. doi:10.1023/A:1007568008032.

Aksu, A.E. 1981. Late Quaternary stratigraphy, paleoenvironmentology, and sedimentation history of Baffin Bay and Davis Strait. Ph. D., Dalhousie University, Halifax, N.S. 771 p.

Aksu, A.E. 1983. Holocene and Pleistocene dissolution cycles in deep-sea cores of Baffin Bay and Davis Strait: paleo-oceanographic implications. Marine Geology, **53**(4): 331–348. doi:10.1016/0025-3227(83)90049-X.

Aksu, A.E., and Piper, D.J.W. 1987. Late Quaternary sedimentation in Baffin Bay. Canadian Journal of Earth Sciences, **24**(9): 1833–1846. doi:10.1139/e87-174.

Alley, R.B., Cuffey, K.M., Evenson, E.B., Strasser, J.C., and Lawson, D.E. 1997. How glaciers entrain and trasnport basal sediment: Physical constraints. Quaternary Science Reviews, **16**(9): 1017–1038. doi:10.1016/S0277-3791(97)00034-6.

Andrews, J.T. 1990. Fiord to deep-sea sediment transfers along the Northeastern Canadian Continental Margin: Models and data. Géographie physique et Quaternaire, **44**: 55–70.

Andrews, J.T. 1993. Changes in the silt- and clay-size mineralogy of sediments at ODP Site 645B, Baffin Bay. Canadian Journal of Earth Sciences, **30**: 2448–2452.

Andrews, J.T. 2000. Icebergs and Iceberg Rafted Detritus (IRD) in the North Atlantic: Facts and Assumptions. Oceanography (Washington, D.C.), **13**: 100–108.

Andrews, J.T., and Freeman, W. 1996. The measurement of sediment color using the colortron spectrophotometer. Arctic and Alpine Research, **28**(4): 524–528. doi:10.2307/1551864.

Andrews, J.T., and MacLean, B. 2003. Hudson Strait ice streams: A review of stratigraphy, chronology, and links with North Atlantic Heinrich events. Boreas, **32**(1): 4–17. doi:10.1080/03009480310001010.

Andrews, J.T., Syvitski, J.P.M., Williams, K.M., Jennings, A.E., Short, S.K., Mode, W.N., and Kravitz, J. 1994. Marine geology of Sunneshine Fiord (Baffin Island). Geological Survey of Canada, Open File Report 3034, 2 sheets.

Andrews, J.T., and Tedesco, K. 1992. Detrital carbonate-rich sediments, northwestern Labrador Sea: Implications for ice-sheet dynamics and iceberg rafting (Heinrich) events in the North Atlantic. Geology, **20**(12): 1087–1090. doi:10.1130/0091-7613(1992)020<1087:DCRSNL>2.3.CO;2.

Andrews, J.T., Buckley, J.T., and England, J.H. 1970. Late-glacial chronology and glacio-isostatic recovery, Home Bay, East Baffin Island, Canada. Geological Society of America Bulletin, **81**(4): 1123–1148. doi:10.1130/0016-7606(1970)81[1123:LCAGRH]2.0.CO;2.

Andrews, J.T., Geirsdottir, A., and Jennings, A.E. 1989a. Late Quaternary spatial and temporal changes in clay- and silt-size mineral assemblages of fiord and shelf cores, western Baffin Island, northwest North Atlantic. Continental Shelf Research, **9**(5): 445–463. doi:10.1016/0278-4343(89)90009-5.

Andrews, J.T., Laymon, C.A., and Briggs, W.M. 1989*b*. Radiocarbon Date List VI, Baffin Island and III Labrador–Ungava. University of Colorado, Boulder, Colo., INSTAAR Occasional Paper No. 46. 85 p.

Andrews, J.T., Osterman, L.E., Jennings, A.E., Syvitski, J.P.M., Miller, G.H., and Weiner, N. 1996. Abrupt changes in marine conditions, Sunneshine Fiord, eastern Baffin Island, N.W.T. (ca. 66°N) during the last deglacial transition: Links to the Younger Dryas cold-event and Heinrich, H-0. *In* Late Quaternary paleoceanography of North Atlantic margins. *Edited by* J.T. Andrews, W. Austin, H. Bergsten, and H.E. Jennings. Geological Society of London. pp. 11–27.

Andrews, J.T., Kirby, M.E., Aksu, A., Barber, D.C., and Meese, D. 1998. Late Quaternary Detrital Carbonate (DC-) layers in Baffin Bay marine sediments (67°–74°N): correlatation with Heinrich Events in the North Atlantic? Quaternary Science Reviews, **17**(2): 1125–1137. doi:10.1016/S0277-3791(97)00064-4.

Andrews, J.T., Kihl, R., Kristjánsdóttir, G.B., Smith, L.M., Helgadóttir, G., Geirsdóttir, Á., and Jennings, A.E. 2002. Holocene sediment properties of the East Greenland and Iceland continental shelves bordering Denmark Strait (64°–68°N), North Atlantic. Sedimentology, **49**(1): 5–24. doi:10.1046/j.1365-3091.2002.00429.x.

Andrews, J.T., Jennings, A.E., Moros, M., Hillaire-Marcel, C., and Eberl, D.D. 2006. Is there a pervasive Holocene ice-rafted debris (IRD) signal in the northern North Atlantic? The answer appears to be either no, or it depends on the proxy! PAGES Newsletter, **14**: 7–9.

Andrews, J.T., Jennings, A.E., Coleman, C.G., and Eberl, D. 2010. Holocene variations in mineral and grain-size composition along the East Greenland glaciated margin (ca 67°–70°N): local versus long-distant sediment transport. Quaternary Science Reviews, **29**(19-20): 2619–2632. doi:10.1016/j.quascirev.2010.06.001.

Azetsu-Scott, K., Clarke, A., Falkner, K., Hamilton, J., Jones, E.P., Lee, C., et al. 2010. Calcium carbonate saturation states in the waters of the Canadian Arctic Archipelago and the Labrador Sea. Journal of Geophysical Research-Oceans, **115**(C11): C11021. doi:10.1029/2009JC005917.

Bigg, G.R. 1999. An estimate of the flux of iceberg calving from Greenland. Arctic, Antarctic, and Alpine Research, **31**(2): 174–178. doi:10.2307/1552605.

Bigg, G.R., Wadley, M.R., Stevens, D.P., and Johnson, J.A. 1996. Prediction of iceberg trajectories for the North Atlantic and Arctic Oceans. Geophysical Research Letters, **23**(24): 3587–3590. doi:10.1029/96GL03369.

Blake, J.W., 1975. Radiocarbon age determination and postglacial emergence at Cape Storm, Southern Ellesmere Island, Arctic Canada. Geografiska Annaler, **57**(1–2): 1–71. doi:10.2307/520528.

Boyd, R.W., and Piper, D.J.W. 1976. Baffin Bay continental shelf clay mineralogy. Maritime Sediments, **21**: 17–18.

Briner, J.P., Miller, G.H., Davis, P.T., Bierman, P.R., and Cafee, M. 2003. Last Glacial Maximum ice sheet dynamics in Arctic Canada inferred from young erratics perched on ancient tors. Quaternary Science Reviews, **22**(5–7): 437–444. doi:10.1016/S0277-3791(03)00003-9.

Briner, J.P., Overseem, I., Miller, G.H., and Finkel, R.C. 2007. The deglaciation of Clyde Inlet, northeastern Baffin Island, Arctic Canada. Journal of Quaternary Science, **22**(3): 223–232. doi:10.1002/jqs.1057.

Campbell, D.C., and de Vernal, A., 2009. CCGS Hudson Expedition 2008029. Marine geology and paleoceanography of Baffin Bay and adjacent areas, Naine, NL to Halifax, NS, August 29 – September 23.

Crane, R.G. 1978. Seasonal variations in sea ice extent in the Davis Strait – Labrador Sea area and relationships with synoptic-scale atmospheric circulation. Arctic, **31**: 434–447.

Davis, J.C. 1986. Statistics and data analysis in geology. John Wiley & Sons, New York, N.Y. 646 p.

Davis, P.T. 1985. Neoglacial moraines on Baffin Island. *In* Quaternary environments: eastern Canadian Arctic, Baffin Bay and western Greenland. *Edited by* J.T. Andrews. Allen and Unwin, London, U.K. pp. 682–718B.

De Angelis, H., and Kleman, J. 2007. Palaeo-ice streams in the Foxe/Baffin sector of the Laurentide Ice Sheet. Quaternary Science Reviews, **26**: 1313–1331.

de Vernal, A., Bilodeau, G., Hillaire-Marcel, C., and Kassou, N. 1992. Quantitative assessment of carbonate dissolution in marine sediments from foraminifer linings vs. shell ratios: Davis Strait, Northwest North Atlantic. Geology, **20**(6): 527–530. doi:10.1130/0091-7613(1992)020<0527:QAOCDI>2.3.CO;2.

Dowdeswell, J.A. 1986. The distribution and character of sediments in a tidewater glacier, Southern Baffin Island, N.W.T., Canada. Arctic and Alpine Research, **18**(1): 45–46. doi:10.2307/1551213.

Dyke, A.S. 2004. An outline of North American deglaciation with emphasis on central and northern Canada. *In* Quaternary glaciations — extent and chronology, Part II. *Edited by* J.A. Ehlers. Elsevier, New York, N.Y. pp. 373–424.

Dyke, A.S., Andrews, J.T., Clark, P.U., England, J.H., Miller, G.H., Shaw, J., and Veillette, J.J. 2002. The Laurentide and Innuitian ice sheets during the Last Glacial Maximum. Quaternary Science Reviews, **21**(1–3): 9–31. doi:10.1016/S0277-3791(01)00095-6.

Eberl, D.D. 2003. User guide to RockJock: A program for determining quantitative mineralogy from X-ray diffraction data. United States Geological Survey, Open File Report 03-78, Washington, D.C. 40 p.

Eberl, D.D. 2004. Quantitative mineralogy of the Yukon River system: Variations with reach and season, and determining sediment provenance. The American Mineralogist, **89**: 1784–1794.

England, J. 1999. Coalescent Greenland and Innuitian ice during the Last Glacial Maximum: revising the Quaternary of the Canadian High Arctic. Quaternary Science Reviews, **18**(3): 421–456. doi:10.1016/S0277-3791(98)00070-5.

Fagel, N., Hillaire-Marcel, C., Humblet, M., Brasseur, R., Weis, D., and Stevenson, R. 2004. Nd and Pb isotope signatures of the clay-size fraction of Labrador Sea sediments during the Holocene: implications for the inception of the modern deep circulation pattern. Palaeoceanography, **19**(3): PA3002. doi:10.1029/2003PA000993.

Farmer, G.L., Barber, D.C., and Andrews, J.T. 2003. Provenance of Late Quaternary ice-proximal sediments in the North Atlantic: Nd, Sr and Pd isotopic evidence. Earth and Planetary Science Letters, **209**(1–2): 227–243. doi:10.1016/S0012-821X(03)00068-2.

Gilbert, R. 1985. Quaternary glaciomarine sedimentation interpreted from seismic surveys of fiords on Baffin Island, N.W.T. Arctic, **38**: 271–280.

Gilbert, R. 1990. Rafting in glacimarine environments. *In* Glacimarine environments: processes and sediments. *Edited by* J.A. Dowdeswell and J.D. Scourse. The Geological Society, London. pp. 105–120.

Gilbert, R., Nielsen, N., Desloges, J.R., and Rasch, M. 1998. Contrasting glacimarine sedimentary environments of two arctic fiords on Disko, West Greenland. Marine Geology, **147**(1-4): 63–83. doi:10.1016/S0025-3227(98)00008-5.

Hanna, E., Huybrechts, P., Steffen, K., Cappelen, J., Huff, R., Shuman, C., et al. 2008. Increased runoff from melt from the Greenland Ice Sheet: A response to global warming. American Meteorological Society, **21**: 331–341. doi:10.1175/2007JCL1964.1171.

Helmke, J.P., Schulz, M., and Bauch, H.A. 2002. Sediment-color record from the Northeast Atlantic reveals patterns of millennial-scale climate variabiluty during the past 500,000 years. Quaternary Research, **57**(1): 49–57. doi:10.1006/qres.2001.2289.

Hesse, R., Rakofsky, A., and Chough, S.K. 1990. The central Labrador Sea: facies and dispersal patterns of clastic sediments in a small ocean basin. Marine and Petroleum Geology, **7**(1): 13–28. doi:10.1016/0264-8172(90)90052-I.

Hillaire-Marcel, C., de Vernal, A., Aksu, A.E., and Macko, S. 1989. High-resolution isotopic and micropaleontological studies of upper Pleistocene sediments at ODP Site 645, Baffin Bay. *In* Proceedings of the ODP, Scientific Results. *Edited by* S.P. Srivastava, M. A. Arthur, B. Clement, et al. Ocean Drilling Program, College Station, Tex. pp. 599–616. doi.10.2973/odp.proc.sr.105.138.1989.

Hiscott, R.N., Aksu, A.E., and Nielsen, O.B. 1989. Provenance and dispersal patterns, Pliocene-Pleistocene section at Site 645, Baffin Bay. *In* Proceedings ODP, scientific results, 105. *Edited by* S.K. Stewart et al. Ocean Drilling Program, College Station, Tex. pp. 31–52.

Holland, D.M., Thomas, R.H., De Young, B., Ribergaard, M.H., and Lyberth, B. 2008. Acceleration of Jakobshavn Isbrae triggered by warm subsurface ocean waters. Nature Geoscience, **1**(10): 659–664. doi:10.1038/ngeo316.

Howat, I.M., Joughin, I., and Scambos, T.A. 2007. Rapid changes in ice discharge from Greenland outlet glaciers. Science, **315**(5818): 1559–1561. doi:10.1126/science.1138478. PMID:17289940.

Hume, M.S. 1972. The distribution of recent foraminifera in southeast Baffin Bay. MSc. thesis, Department of Oceanography, Dalhousie University, Halifax, N.S., Canada. 137 p.

Jackson, G.D., and Berman, R.G. 2000. Precambrian metamorphic and tectonic evolution of northern Baffin Island, Nunavut, Canada. Canadian Mineralogist, **38**(2): 399–421. doi:10.2113/gscanmin.38.2.399.

Jacobs, J.D., Andrews, J.T., and Funder, S. 1985. Environmental background. *In* Quaternary environments: eastern Canadian Arctic, Baffin Bay and western Greenland. *Edited by* J.T. Andrews. Allen and Unwin, Boston, Mass. pp. 26–68.

Jennings, A.E. 1993. The quaternary history of Cumberland Sound, Southeastern Baffin Island: The marine evidence. Géographie physique et Quaternaire, **47**: 21–42.

Kilfeather, A., O'Cofaigh, C., Jennings, A.E., Dowdeswell, J.A., Quentin, S., and Walton, M. 2010. Holocene glacimarine sedimentation associated with a major West Greenland ice stream: facies analysis of cruise JR175 Disko Bught cores. *In* 40th International Arctic Workshop, Abstract with Program, Winter Park, Colo. INSTAAR, University of Colorado. p. 113.

Knudsen, K.L., Stabell, B., Seidenkrantz, M.S., Eiriksson, J., and Blake, W., Jr. 2008. Deglacial and Holocene conditions in northernmost Baffin Bay: sediments, foraminifera, diatoms and stable isotopes. Boreas, **37**(3): 346–376. doi:10.1111/j.1502-3885.2008.00035.x.

Kovach Computing Services. 1998. Multi-variate statistical package. Kovach Computing Services, Pentraeth, Wales. 127 p.

Kranck, K. 1966. Sediments of Exeter Bay, Baffin Island, District of Franklin. Geological Survey of Canada, Paper 66-8. 60 p.

Kravitz, J.H. 1976. Textural and mineralogical characteristics of the surficial sediments of Kane Basin. Journal of Sedimentary Petrology, **46**: 710–725.

Kravitz, J.H. 1982. Sediments and sediment processes in Kane Basin, a high arctic glacial marine basin. University of Colorado, Boulder, Colo., INSTAAR Occasional Paper No. 39. 184 p.

Kravitz, J.H., and Sorensen, F.H. 1970. Sedimentological reconnaissance survey of Kane Basin. Maritime Sediments, **6**: 17–20.

Kwok, R., Pedersen, L.T., Gudmandsen, P., and Pang, S.S. 2010. Large sea ice outflow into the Nares Strait in 2007. Geophysical Research Letters, **37**(3): L03502. doi:10.1029/2009GL041872.

MacLean, B. 1985. Geology of the Baffin Island Shelf. Allen and Unwin, London, UK. pp. 154–177.

MacLean, B. (*Editor*). 2001. Bedrock geology of Hudson Strait and Ungava Bay. *In* Marine Geology of Hudson Strait and Ungava Bay, Eastern Arctic Canada: Late Quaternary sediments, depositional environments, and late glacial-deglacial history derived from marine and terrestrial studies. Queen's Printer, Ottawa, Ont. Geological Survey of Canada, Bulletin 566. pp. 65–69.

MacLean, B., Williams, G.L., Sanford, B.V., Klassen, R.A., Blakeney, C., and Jennings, A.E. 1986. A reconnaissance of the bedrock and surficial geology of Hudson Strait. Preliminary results. Geological Survey of Canada, Paper 86-1B. pp. 617–635.

MacLean, B., Williams, G.L., and Srivasatava, S.P. 1990. Geology of rthe Labrtador Shelf, Baffin Bay, and Davis Strait. Part 2. Geology of Baffin Bay and Davis Strait. *In* Geology of the continental margin of eastern Canada. *Edited by* M.J. Keen and G.L. Williams. Canadian Government Publishing Center, Ottawa, Ont., Geology of Canada, No. 2. pp. 293–348.

Marlowe, J.I. 1966. Mineralogy as an indicator of long-term current fluctuations in Baffin Bay. Canadian Journal of Earth Sciences, **3**: 191–201.

Marshall, S.J., Clarke, G.K.C., Dyke, A.S., and Fisher, D.A. 1996. Geologic and topographic controls on fast flow in the Laurentide and Cordilleran Ice Sheets. Journal of Geophysical Research, **101** (B8): 17 827 – 17 839. doi:10.1029/96JB01180.

McCarty, D.K. 2002. Quantitative mineral analysis of clay-bearing mixtures: The "Reynolds Cup" contest. International Union of Crystallography, Newsletter, **27**: 12–16.

McCave, I.N., Hall, I.R., and Bianchi, G.G. 2006. Laser vs. settling velocity differences in silt grainsize measurements: estimation of palaeocurrent vigour. Sedimentology, **53**(4): 919–928. doi:10.1111/j.1365-3091.2006.00783.x.

O'Cofaigh, C., and Party, J.S. 2009. RRS James Clark Ross Cruise Report — JR175 West Greenland and Baffin Bay. Marine geophysical and geological investigations of past flow stability of a major Greenland ice stream in the late Quaternary. Department of Geography, Durham, UK.

O'Cofaigh, C., Evans, D.J.A., and Smith, I.R. 2010. Large-scale reorganization and sedimentation of terrestrial ice streams during late Wisconsinan Laurentide Ice Sheet deglaciation. Geological Society of America Bulletin, **122**: 743–756.

Ortiz, J.D., Polyak, L., Grebmeier, J.M., Darby, D., Eberl, D., Naidu, S., and Nof, D. 2009. Provenance of Holocene sediment on the Chukchi–Alaskan margin based on combined diffuse spectral reflectance and quantitative X-ray diffraction analysis. Global and Planetary Change, **68**: 71–84.

Osterman, L.E., and Nelson, A.R. 1989. Latest Quaternary and Holocene paleoceanography of the eatern Baffin Island continental shelf, Canada: benthic foraminiferal evidence. Canadian Journal of Earth Sciences, **26**: 2236–2248.

Paillard, D., Labeyrie, L., and Yiou, P. 1996. Macintosh program performs time-series analysis. EOS, **77**(39): 379. doi:10.1029/96EO00259.

Parnell, J., Bowden, S., Taylor, C., and Andrews, J.T. 2007. Biomarker determination as a provenance tool for detrital carbonate events (Heinrich events?): Fingerprinting Quaternary glacial sources in Baffin Bay. Earth and Planetary Science Letters, **257**(1–2): 71–82. doi:10.1016/j.epsl.2007.02.021.

Piper, D.J.W. 1973. A late quaternary stratigraphic marker in the Central Basin of Baffin Bay. Maritime Sediments, **9**: 62–63.

Piper, D.J.W., and Slatt, R.M. 1977. Late Quaternary clay mineral distribution on the eastern continental margin of Canada. Geological Society of America Bulletin, **88**(2): 267–272. doi:10.1130/0016-7606(1977)88<267:LQCDOT>2.0.CO;2.

Praeg, D.B., MacLean, B., and Sonnichsen, S. 2006. Quaternary geology of the Northeast Baffin Island continental shelf, Cape Aston to Buchan Gulf (70° to 72°N). Geological Survey of Canada, Open File 5409. 92 p.

Ramsey, C.B. 2008. Deposition models for chronological records. Quaternary Science Reviews, **27**(1–2): 42–60. doi:10.1016/j.quascirev.2007.01.019.

Reeh, N. 1994. Workshop on the calving rates of west Greenland glaciers in response to climate change: Danish Polar Center. Mimeo Report.

Reid, C.M., James, N.P., Kyser, T.K., and Beauchamp, B. 2008. Diagenetic cycling of nutrients in seafloor sediments and the carbonate–silica balance in a Paleozoic cool-water carbonate system, Sverdrup Basin, Canadian Arctic Archipelago. Journal of Sedimentary Petrology, **78**(8): 562–578. doi:10.2110/jsr.2008.057.

Schmith, T., and Hansen, C. 2003. Fram Strait ice export during the nineteenth and twentieth centuries reconstructed from a multiyear sea ice index from Southwestern Greenland. Journal of Climate, **16**(16): 2782–2791. doi:10.1175/1520-0442(2003)016<2782:FSIEDT>2.0.CO;2.

Skaarup, N., Jackson, H.R., and Oakey, G. 2006. Margin segmentation of Baffin Bay/Davis Strait, eastern Canada based on seismic reflection and potential field data. Marine and Petroleum Geology, **23**(1): 127–144. doi:10.1016/j.marpetgeo.2005.06.002.

Smith, L.M., and Licht, K.J. 2000. Radiocarbon Date List IX: Antarctica, Arctic Ocean, and the Northern North Atlantic. University of Colorado, Boulder, Colo., INSTAAR Occasional Paper No. 54. 138 p.

Srivastava, S.P., Arthur, M., Clement, B., et al. 1987. Part A — Initial Reports Sites 645–647 Baffin Bay and Labrador Sea. Ocean Drilling Program, Texas A & M University, Washington, D.C. 917 p.

Srivastava, S.P., Arthur, M.A., Clement, B., et al. 1989. Scientific Results Baffin Bay and Labrador Sea. Ocean Drilling Program, Texas A & M University, Washington, D.C. 1038 p.

Syvitski, J.P.M. 1989. On the deposition of sediment within glacier-influenced fjords. Oceanographic controls. Marine Geology, **85**(2–4): 301–329. doi:10.1016/0025-3227(89)90158-8.

Syvitski, J.P.M., and Blakeney, C.C. 1983. Sedimentology of Arctic Fjords Experiment: HU82-031. Canadian Data Report on Hydrography and Ocean Sciences 12. 935 p.

Syvitski, J.P.M., and Hein, F.J. 1991. Sedimentology of an Arctic basin: Itirbilung Fiord, Baffin Island, Northwest Territories. Geological Survey of Canada, Paper 91-11. 66 p.

Syvitski, J.P.M., Andrews, J.T., and Dowdeswell, J.A. 1996a. Sediment deposition in an iceberg-dominated Glacimarine Environment, East Greenland: Basin Fill Implications. Global and Planetary Change, **12**(1–4): 251–270. doi:10.1016/0921-8181(95)00023-2.

Syvitski, J.P.M., Lewis, C.F.M., and Piper, D.J.W. 1996*b*. Paleoceanographic information derived from acoustic surveys of glaciated continental margins: examples from eastern Canada. *In* Late Quaternary paleoceanography of the North Atlantic margins. *Edited by* J.T. Andrews, W. Austin, H. Bergsten, and H.E. Jennings. Geological Society, London, UK. pp. 51–76.

Syvitski, J.P., et al. 1998. Plume 1.1: Deposition of sediment from a fluvial plume. Computers & Geosciences, **24**(2): 159–171. doi:10.1016/S0098-3004(97)00084-8.

Tang, C.C.L., Ross, C.K., Yao, T., Petrie, B., Detracey, B., and Dunlap, E. 2004. The circulation, water masses and sea-ice of Baffin Bay. Progress in Oceanography, **63**(4): 183–228. doi:10.1016/j.pocean.2004.09.005.

Thiebault, F., Cremer, M., Debraband, P., Foulon, J., Nielsen, O.B., and Zimmerman, H. 1989: Analysis of sedimentary facies, clay mineralogy, and geochemistry of the Neogene-Quaternary sediments in ODP Site 645, Baffin Bay. *In* Proceedings ODP, science results,

105. *Edited by* S.P. Srivastava, M.A. Arthur, B. Clement, et al. Ocean Drilling Program, College Station, Tex. pp. 83–100.

Tippett, C.R. 1985. Glacial dispersal train of Paleozoic erratics, central Baffin Island, N.W.T., Canada. Canadian Journal of Earth Sciences, **22**: 1818–1826.

Trask, P.D. 1932. The sediments. *In* The "Marion" expedition to Davis Strait and Baffin Bay under direction of the United States Coast Guard, 1928; scientific results Part 1; the bathymetry and sediments of Davis Strait. *Edited by* N.G. Rickets and P.D. Trask. United States Government Printing Office, Washington, D.C. pp. 62–81.

Walden, J. 1999. Remanence measurements. *In* Environmental magnetism: a practical guide. *Edited by* J. Walden, F. Oldfield, and J. Smith. Quaternary Research Association, London, UK. pp. 63–88.

Walden, J., Oldfield, F., and Smith, J. 1999. Environmental magnetism: A practical guide. Quaternary Research Association, London, UK. 243 p.

Weidick, A., and Bennike, O. 2007. Quaternary glaciation history and glaciology of Jakobshavn Isbrae and the Disko Bugt region, West Greenland: a review. Geological Survey of Denmark and Greenland, Bulletin 14. 80 p.

Appendix A

Surface sample latitudes and longitudes.

Table A1. Surface sample locations (Fig. 1) and relationship to Fig. 5.

Series (see Fig. 5)	Site id	PCA cluster	Longitude	Latitude	Water depth
1	HU2008029-24	3	–74.343	77.288	728
2	HU64090-30	1	–74.083	77	441
3	HU2008029-28	3	–71.891	76.979	1 048
4	HU64090-31	2	–74.083	76.667	590
5	HU2008029-37	3	–73.955	76.573	680
6	3HU2008029-36	3	–71.421	76.329	680
7	HU64090-32	2	–70.5	76.233	649
8	HU64090-33.B	2	–71.4	76.158	570
9	HU64090-34	1	–72.358	76.129	485
10	HU64090-35	1	–74.383	76.033	354
11	HU64090-35.1	2	–73.167	76	395
12	HU64090-48.13	1	–71.05	75.925	426
13	HU64090-35.5	1	–69.333	75.8	470
14	HU64090-48	1	–66.55	75.8	580
15	HU64090-36	1	–68.467	75.75	403
16	HU64090-48.1	1	–67.283	75.717	348
17	HU64090-48.12	1	–71.4	75.667	512
18	HU64090-47.1	1	–67	75.65	440
19	HU64090-37	2	–70.083	75.617	521
20	HU2008029-40	3	–78.629	75.579	580
21	6HU64090-37.1	2	–71	75.55	583
22	* HU2008029-19	1	–70.635	75.469	602
23	HU64090-38	2	–71.867	75.467	598
24	HU64090-48.3	1	–69.083	75.467	535
25	HU64090-48.11	2	–71.85	75.447	586
26	HU64090-39	2	–73.567	75.392	550
27	HU64090-48.4	2	–69.917	75.337	645
28	HU64090-39.1	2	–74.45	75.283	480
29	HU64090-46.1	1	–68.083	75.233	620
30	HU64090-40	2	–75.3	75.217	417
31	HU64090-48.5	2	–70.742	75.203	630
32	HU64090-48.9	2	–72.717	75.008	743
33	HU64090-48.7	2	–72.333	74.933	823
34	HU64090-45.3R	2	–69.633	74.783	1 426
35	HU64090-54	3	–67.75	74.767	1 940
36	HU64090-50.4	3	–73.783	74.717	669
37	HU64090-50.2	2	–75.85	74.63	558
38	HU64090-50.6	2	–72	74.617	1 111
39	HU64090-50.7	2	–71	74.55	1 291
40	HU64090-53	3	–70.15	74.433	1 530
41	HU64090-45	2	–72.133	74.133	1 006
42	HU2008029-55	3	–78.719	74.092	866
43	HU2008029-47	3	–77.116	74.023	870
44	HU64090-44.1	2	–73.083	73.95	848
45	HU64090-44	2	–74.133	73.783	858
46	HU77024–18	1	–66.998	73.7	2 365
47	HU77024–26	2	–70.483	73.7	1 463
48	HU77024–17	3	–64.562	73.688	1 500
49	* HU2008029-66	3	–67.878	72.434	2 357
50	HU2008029-63	3	–67.717	72.406	2 375
51	HU77024-19	2	–65.972	72.202	2 323
52	HU80026-9	3	–73.233	71.892	585
53	HU80026-10	3	–72.84	71.878	627

Table A1 (*concluded*).

Series (see Fig. 5)	Site id	PCA cluster	Longitude	Latitude	Water depth
54	HU77027-7	1	–73.163	71.848	562
55	HU82028-70	1	–70.025	71.605	238
56	HU82028-14	3	–70.207	71.512	660
57	HU82028–25	1	–70.392	71.497	590
58	HU82028-27	3	–70.43	71.465	680
59	HU82028-21	1	–70.14	71.457	594
60	HU82028-30	1	–70.225	71.453	547
61	HU82028-29	1	–70.338	71.44	631
62	HU82028-43	3	–70.407	71.417	703
63	HU82028-42	3	–70.365	71.413	695
64	HU82028-41	3	–70.302	71.39	677
65	HU72024-17	3	–70.383	71.333	622
66	JC175VC40	1	–53.436	71.278	663
67	JC175VC42	1	–56.092	70.882	554
68	JC175VC43	1	–59.621	70.623	629
69	* HU2008–14	2	–64.657	70.461	2 060
70	34390- 0	3	–53.052	70.22	537
71	34390-10	3	–53.053	70.219	538
72	* JC175BC06	3	–63.06	69.933	2 034
73	DA06-26 cm	1	–51.395	69.17	363
74	HU2008029-079TWC	1	–65.633	68.875	
75	JC175VC29	1	–55.543	68.499	400
76	343300	1	–54.001	68.47	518
77	* JR175-BC01	3	–55.898	68.398	545
78	* HU2008029-68	1	–57.618	68.228	437
79	HU2008-029-070	1	–57.617	68.227	444
80	HU77024–12	2	–61.335	68.12	1 682
81	HU80026-80	1	–63.292	67.843	362
82	HU82-SU5	3	–61.71	66.556	155

*Box core.

Appendix B. AutoMinUnMix v3

This program is a modified version of MinUnMix (Eberl 2004) — the program is available from dderbl@usgs.gov. Input consists of (1) names of the mineral species; (2) composition of between 1 to 6 source compositions, summing to 100%; and (3) individual site or down core compositions. The program uses the Solver™ in Excel to iteratively seek for a solution that minimizes the degree-of-fit, defined as DOF = sum abs value (measured-calc)/100, where 100 = normalized sum measured. The average departure or difference (AD%) is defined as AD% = Sum | observed wt.% – estimated wt.%|/number of species. The relationship between DOF and AD% is simply AD% = DOF*k, where k is 100/number of mineral species. The solution for each sample is accepted when the convergence estimates do not differ from 0.0001 over five steps. An example of the Output under Worksheet "Results" is shown in Table B1.

A substantial upgrade to the MinUnMix program has recently been implemented. This version is now called "SedUnMix" (sediment unmixing) and is available from ftp://brrcrftp.cr.usgs.gov/pub/ddeberl/.

Table B1. Output under Worksheet results.

Reference No.:	1	2	3
Sample end members (depth in cm, JR175BC06)	0	2	4
Umanak	0.39	0.00	0.46
Ebaffin	0.18	0.45	0.08
Nbaffin	0.15	0.20	0.01
Jak	0.14	0.20	0.36
SUM (%):	85.56	85.62	90.21
Degree-of-fit:	0.41	0.40	0.42
Average deviation:	2.05	2.00	2.11
Minerals present	Average deviation	Average deviation	Average deviation
Ordered microcline feldspar	1.1	1.8	2.1
Intermediate microcline feldspar	3.6	0.7	3.5
Orthoclase feldspar	2.6	2.1	1.2
Anorthoclase feldspar	5.1	0.0	4.3
Albite feldspar (cleavelandite)	0.4	2.3	0.3
Oligoclase feldspar (Norway)	0.0	1.1	1.4
Labradorite feldspar	0.1	2.7	0.0
Amphibole (ferrotschermakite)	0.3	0.3	0.5
Pyroxene (diopside)	2.0	0.1	2.6
Maghemite	0.7	0.8	0.7
Chert (8.4 nm)	0.0	6.1	0.0
Kaolinite (dry branch)	1.7	2.6	2.5
Saponite	3.0	5.8	3.1
Ferruginous smectite	1.7	2.5	2.1
1Md illite (+ dioct mica and smectite)	4.1	0.3	4.6
1M Illite (R > 2; 88% I)	8.0	2.8	7.8
1M illite (R > 1, 70%–80% I)	3.8	1.6	3.3
Biotite (1M)	0.9	5.2	0.6
Fe-chlorite (Tusc)	2.0	1.3	1.6
Muscovite (2M1)	0.0	0.0	0.0

Note: The program also produces graphs of the difference between the observed and estimated wt.% at each level (e.g., Fig. 10).